*Journal of Sound and Vibration* (2002) **252**(5), 883–918
doi:10.1006/jsvi.2001.3833, available online at http://www.idealibrary.com on IDEAL®

# VORTEX–SURFACE INTERACTION NOISE: A COMPENDIUM OF WORKED EXAMPLES

H. Abou-Hussein, A. DeBenedictis, N. Harrison, M. Kim, M. A. Rodrigues, F. Zagadou and M. S. Howe

*College of Engineering, Boston University*, 110 *Cummington Street, Boston Massachusetts* 02215, *U.S.A. E-mail: mshowe@bu.edu*

(*Received* 1 *February* 2001, *and in final form* 16 *May* 2001)

Students attending a graduate course on the *Theory of Vortex Sound* given recently at Boston University were required to investigate the low Mach number unsteady flow and the accompanying acoustic radiation for a selection of idealized flow–structure interactions. These included linear and non-linear parallel blade–vortex interactions for two-dimensional airfoils, and for finite span airfoils of variable chord; interactions between line vortices and surface projections from a plane wall; bluff-body interactions involving line and ring vortices impinging on circular cylindrical and spherical bodies, and vortex motion in the neighborhood of a wall aperture. In all cases, the effective source region was localized in either two or three dimensions, and could be regarded as acoustically compact, and the sound was calculated by routine numerical methods using the theory of compact Green functions. The results are collected together in this paper as a compendium of canonical solutions that provide qualitative and quantitative insight into the mechanisms responsible for sound production, and a database that can be used to validate predictions of more generally applicable numerical schemes. 

## 1. INTRODUCTION

Lighthill's "acoustic analogy" [1] expresses the equivalence of sound production by a flow and the generation of sound in an ideal, stationary medium driven predominantly by the Reynolds stress fluctuations. In a homentropic medium, the theory can be recast into a form where vorticity alone may be identified as the ultimate "source" of sound [2–4]. Lighthill was a strong advocate of the study of vorticity for analyzing complex flows ("the only quantity whose variations are not propagated at the enormous speed of sound" [5]), and pioneered in the late 1950s the "vortex method" for the numerical solution of unsteady flows. This has since become one of the major tools for investigating complex flow–structure interactions at low Mach numbers [6, 7], and also provides the most efficient means of calculating the accompanying acoustic noise. Vortex–airfoil interactions constitute a particularly important subclass of such flows, and the literature contains many accounts of their numerical simulation (e.g., references [8–13]) and predictions of the sound they produce.

Students attending a recent graduate level course on the *Theory of Vortex Sound* at Boston University were required to investigate the interaction at low Mach number of idealized vortex structures (rectilinear or circular line vortices) with several simple solid boundaries, and to calculate the sound generated by the interactions. These included (1) blade–vortex interactions in two dimensions, (2) parallel blade–vortex interactions in three dimensions, (3) a vortex interacting with a wall barrier, (4) a vortex interacting with

0022-460X/02/$35.00 

a circular cylinder, (5) line and ring vortices interacting with a sphere, and (6) a vortex pair incident on a wall aperture.

Some of these are too idealized to be representative of real flow–structure interactions, but all of them can be regarded as special limiting cases, and the resulting noise predictions can assist in the validation of more generally applicable numerical schemes. In addition, whereas the results of each separate calculation might not be especially significant, a compilation of predictions for the whole set provides valuable insight into the mechanisms of sound generation by flow–structure interactions at low Mach numbers. Therefore, in this paper the results of the student projects are gathered together into a compendium of predictions with the dual purpose of providing a reference set of analytical predictions and a tutorial on mechanisms of sound production by vortex–surface interactions. Most of these interactions have been considered previously in the literature, in various forms and approximations, and specific references to earlier work are given later in the paper.

The relevant standard formulae and equations of the theory of vortex sound are reviewed in section 2, in forms suitable for application to both two- and three-dimensional interactions. The remaining sections of the paper are devoted to discussions of problems (1)–(6). In all cases, the Mach number is assumed to be sufficiently small so that the details of the vortex–surface interaction can first be determined by taking the motion to be incompressible. The predicted rotational flow is then used to calculate the radiated sound using the appropriate compact Green function (also discussed in section 2) tailored to the surface geometry.A novel alternative to the usual application of the unsteady Kutta condition is used in problems (1) and (2) to model the influence of additional vorticity shed from an edge [14]. It was desirable that student projects could be successfully completed by relatively elementary means, without the need to explicitly evaluate the properties of a vortex wake (in contrast to the classical airfoil–gust interaction problem of Sears [15]). A formal procedure was adopted that is strictly valid at *high reduced frequencies*, when the hydrodynamic wavelength of the flow is small compared to the airfoil chord. This method identifies the principal locations of flow–structure interaction noise sources with singularities of the compact Green function, which for an airfoil occur in the vicinities of the leading and trailing edges. Vortex shedding from an edge induced by an incident "gust" is known to *reduce* the importance of that edge in generating sound [4]. Because the edges behave as independent sources at high reduced frequencies, the trailing edge source can be removed essentially by deleting the corresponding edge singularity from the Green function. The accuracy of this procedure is discussed in section 3, where a comparison with predictions based on the full Sears analysis indicates that the approximation is valid for vortex length scales as large as the airfoil chord.

## 2. VORTEX–SURFACE INTERACTION NOISE AT LOW MACH NUMBERS

To cast Lighthill's theory of aerodynamic sound into a form in which vorticity is identified as the ultimate source, it is necessary to adopt the *total enthalpy B* as the acoustic variable, as opposed to the pressure $p$ or density $\rho$. The source terms in the reformulated theory are then confined to those regions where the vorticity $\boldsymbol{\omega} \neq \mathbf{0}$ and where $\nabla s \neq \mathbf{0}$, where $s$ is the entropy. In many applications (for example, in the absence of combustion), it is permissible to regard the source flow as *homentropic*. Then Lighthills' equations takes the form [3, 4]

$$\left(\frac{D}{\mathrm{D}t}\left(\frac{1}{c^2}\frac{\mathrm{D}}{\mathrm{D}t}\right) - \frac{1}{\rho}\nabla\cdot(\rho\nabla)\right) B = \frac{1}{\rho}\,\mathrm{div}\,(\rho\omega \wedge \mathbf{v}), \tag{1}$$

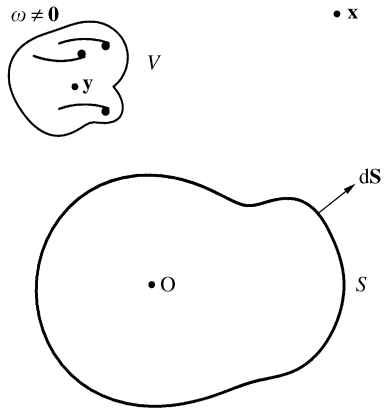


Figure 1. Low Mach number vortical flow in the vicinity of a rigid body $S$.

where $c$ is the local speed of sound and $\mathbf{v}$ is the velocity. Bernoulli's equation implies that in the absence of vorticity and moving boundaries the total enthalpy

$$B = \int \frac{\mathrm{d}p}{\rho} + \frac{1}{2} v^2 \tag{2}$$

is a constant that may be assumed to vanish. Outside the source flow the unsteady motion is entirely irrotational with velocity potential $\varphi(\mathbf{x}, t)$, say, and $B = -\partial\varphi/\partial t$, so that $B$ is easily related to the acoustic pressure in the far field. If the fluid is assumed to be at rest at infinity the acoustic pressure $p = \rho_0 B$, where $\rho_0$ is the uniform mean density in the far field.

The left side of the vortex sound equation (1) takes explicit account of non-linear effects on propagation, because the local values of the density $\rho$, sound speed $c$ and the flow velocity $\mathbf{v}$ all occur in the differential wave operator. In an extensive region of turbulence, whose size exceeds many characteristic acoustic wavelengths, or where a mean shear layer contributes a large *linear* contribution to $\boldsymbol{\omega} \wedge \mathbf{v}$, the scattering and refraction within the source region can also be important, this effect is implicitly included in the source term.

An important subclass of problems involves unsteady, low Mach number vortical flow in the neighborhood of a stationary rigid body $S$, in the vicinity of which the motion may be regarded as incompressible (Figure 1). When non-linear effects on the *propagation* of the aerodynamic sound are also ignored, and the mean flow is at rest at infinity (if necessary by means of a suitable Galilean transformation) equation (1) reduces to the much simplified form

$$\left(\frac{1}{c_0^2}\frac{\partial^2}{\partial t^2} - \nabla^2\right) B = \operatorname{div}(\boldsymbol{\omega} \wedge \mathbf{v}), \tag{3}$$

where the speed of sound $c_0$ may now be regarded as constant.

This equation can be solved by introducing a Green function $G(\mathbf{x}, \mathbf{y}, t - \tau)$ that satisfies

$$\left(\frac{1}{c_0^2}\frac{\partial^2}{\partial \tau^2} - \frac{\partial^2}{\partial y_j^2}\right) G = \delta(\mathbf{x} - \mathbf{y})\,\delta(t - \tau), \quad G = 0 \text{ for } \tau > t \tag{4}$$

and has vanishing normal derivatives $\partial G/\partial x_n$, $\partial G/\partial y_n$, respectively, for $\mathbf{x}$ and $\mathbf{y}$ on $S$. The application of the Green theorem then permits the solution of equation (3) to be cast in the form [4, 16, 17]

$$B(\mathbf{x}, t) \approx -\int_V (\boldsymbol{\omega} \wedge \mathbf{v})_j (\mathbf{y}, \tau) \frac{\partial G}{\partial y_j}(\mathbf{x}, \mathbf{y}, t-\tau)\, \mathrm{d}^3\mathbf{y}\, \mathrm{d}\tau + \nu \oint_S \boldsymbol{\omega}(\mathbf{y}, \tau) \wedge \frac{\partial G}{\partial \mathbf{y}}(\mathbf{x}, \mathbf{y}, t-\tau) \cdot \mathrm{d}\mathbf{S}(\mathbf{y})\, \mathrm{d}\tau, \tag{5}$$

where $\nu$ is the kinematic viscosity, and the momentum equation has been used in Crocco's form [4],

$$\frac{\partial \mathbf{v}}{\partial t} + \nabla B = -\boldsymbol{\omega} \wedge \mathbf{v} - \nu \operatorname{curl} \boldsymbol{\omega}$$

with the neglect of dilatational viscous terms in the source region.

Let us now specialize the discussion to cases where the body $S$ is acoustically *compact* (or, for an airfoil-like structure, where the *chord* is compact). According to Curle's [18] extension of Lighthill's theory, solution (5) is equivalent to that generated by a *dipole* acoustic source whose strength is proportional to the net unsteady force exerted on the fluid by the body. An explicit representation of this dipole sound is obtained by using the *compact* approximation to the Green function [3, 4],

$$G(\mathbf{x}, \mathbf{y}, t-\tau) = \frac{1}{4\pi|\mathbf{X}-\mathbf{Y}|}\, \delta\left(t - \tau - \frac{|\mathbf{X}-\mathbf{Y}|}{c_0}\right). \tag{6}$$

The vector $\mathbf{Y} = (Y_1(\mathbf{y}),\ Y_2(\mathbf{y}),\ Y_3(\mathbf{y}))$ in this formula will be referred to as the *Kirchhoff vector* of the body; it is defined by

$$Y_i(\mathbf{y}) = y_i - \varphi_i^*(\mathbf{y}), \tag{7}$$

where $\varphi_i^*(\mathbf{y})$ is the velocity potential of ideal incompressible flow that would be produced by motion of $S$ at unit speed in the $i$ direction.

The potential functions $\varphi_i^*(\mathbf{y})$ were introduced by Kirchhoff (see section 2.9 of reference [19] for a detailed discussion). They are a geometrical property of $S$, and satisfy

$$n_j \frac{\partial \varphi_i^*}{\partial y_j} = n_i \text{ on } S \quad \text{and} \quad \nabla\varphi_i^* \sim O\left(\frac{1}{|\mathbf{y}|^3}\right) \text{as } |\mathbf{y}| \to \infty,$$

where $\mathbf{n}$ is the unit normal on $S$ (directed into the fluid). They are usually associated with the definition of the *added mass* tensor [19],

$$M_{ij} = M_{ji} = -\rho_0 \oint_S n_j \varphi_i^*\, \mathrm{d}S \equiv -\rho_0 \oint_S n_i \varphi_j^*\, \mathrm{d}S.$$

The Kirchhoff vector $\mathbf{Y}(\mathbf{y})$ is therefore determined by the shape of $S$. $Y_i(\mathbf{y})$ is just the velocity potential of ideal flow past $S$ having unit speed in the $i$ direction at large distances from $S$; the normal derivative $\partial Y_i/\partial y_n = 0$ on $S$. The function $\mathbf{X}(\mathbf{x})$ in equation (6) is defined similarly in terms of $\mathbf{x}$.

The compact Green function (6) is an approximate solution of equation (4) that agrees with the exact Green function when the latter is expanded in a multipole series and all terms of quadrupole order and higher are discarded; representation (6) is valid provided *either* $\mathbf{x}$ or $\mathbf{y}$ lies in the far field of the body. When $\mathbf{x}$ lies in the acoustic far field, and $S$ is

a three-dimensional compact body, the expansion of $G$ to dipole order in the retarded time yields

$$G(\mathbf{x}, \mathbf{y}, t-\tau) \approx \frac{1}{4\pi|\mathbf{x}|}\left(\delta(t-\tau-|\mathbf{x}|/c_0) + \frac{x_j Y_j}{c_0|\mathbf{x}|}\,\delta'(t-\tau-|\mathbf{x}|/c_0)\right), \quad |\mathbf{x}| \to \infty, \tag{8}$$

where the prime denotes differentiation with respect to $t$. Only the second term in this expansion makes a non-zero contribution when substituted into the right-hand side of the general solution (5). Thus, recalling that $B \sim p/c_0$ in the acoustic far field, this procedure supplies the dipole acoustic pressure in the form

$$p(\mathbf{x}, t) \approx -\frac{x_j}{4\pi c_0|\mathbf{x}|^2}\frac{\partial}{\partial t}\left[\rho_0 \int_V \nabla Y_j \cdot \boldsymbol{\omega} \wedge \mathbf{v}\, \mathrm{d}^3\mathbf{y} + \eta \oint_S \nabla Y_j \cdot \boldsymbol{\omega} \wedge \mathrm{d}\mathbf{S}\right], \quad |\mathbf{x}| \to \infty, \tag{9}$$

where $\eta = \rho_0 \nu$ is the shear coefficient of viscosity, and the terms in square braces [ ] are evaluated at the retarded time $t - |\mathbf{x}|/c_0$. The integrals, respectively, represent the dipole strengths produced by the normal stresses on $S$ generated by the freefield vorticity and by the surface frictional forces. The latter is usually discarded at very large Reynolds numbers, in which case we can write

$$p(\mathbf{x}, t) \approx \frac{-\rho_0 x_j}{4\pi c_0|\mathbf{x}|^2}\frac{\partial}{\partial t}\int (\boldsymbol{\omega} \wedge \mathbf{v})\left(\mathbf{y}, t - \frac{|\mathbf{x}|}{c_0}\right) \cdot \nabla Y_j(\mathbf{y})\, \mathrm{d}^3\mathbf{y}, \quad |\mathbf{x}| \to \infty. \tag{10}$$

In this paper, we shall also discuss applications of the simplified vortex sound equation (3) to vortex–surface interaction problems in two dimensions, involving a *cylindrical* body $S$ whose generators are parallel to the $x_3$-axis of the co-ordinate system $(x_1, x_2, x_3)$, when the motion is constant in planes parallel to $x_3 = 0$. The vortex sound source $\boldsymbol{\omega} \wedge \mathbf{v}$ is then independent of $x_3$, and $\omega_3$ is the only non-zero component of the vorticity. The Green function for cylindrical $S$ of *compact cross-section* is still given by equation (6) where now, however, the Kirchoff vectors $\mathbf{X}$ and $\mathbf{Y}$ reduce to

$$X_{1,2} = x_{1,2} - \varphi^*_{1,2}(\mathbf{x}), \quad Y_{1,2} = y_{1,2} - \varphi^*_{1,2}(\mathbf{y}), \qquad X_3 = x_3, \quad Y_3 = y_3.$$

Thus, $G(\mathbf{x}, \mathbf{y}, t-\tau)$ is a function of $x_3 - y_3$, and this implies that the corresponding *two-dimensional* compact Green function, which satisfies equation (4) when the right side is replaced by

$$\delta(x_1 - y_1)\delta(x_2 - y_2)\delta(t-\tau),$$

can be derived by integrating the three-dimensional formula (6) over $-\infty < y_3 < \infty$ (Hadamard's "method of descent" [20]). The integration simplifies when $\mathbf{x}$ lies in the far field of the cylinder. The "monopole" part of the resulting expression is independent of $\mathbf{y}$ and may be discarded (because it makes no contribution to the radiation generated by the divergence source $\mathrm{div}(\boldsymbol{\omega} \wedge \mathbf{v})$), in which case we find

$$G(\mathbf{x}, \mathbf{y}, t-\tau) \approx \frac{\mathbf{x}\cdot\mathbf{Y}}{2\pi\sqrt{2c_0}|\mathbf{x}|^{3/2}}\frac{\partial}{\partial t}\left\{\frac{\mathrm{H}(t-\tau-|\mathbf{x}|/c_0)}{\sqrt{t-\tau-|\mathbf{x}|/c_0}}\right\}, \quad |\mathbf{x}| \to \infty, \tag{11}$$

where $\mathbf{x} = (x_1, x_2)$, $\mathbf{Y} = (Y_1, Y_2)$, and H is the Heaviside step function.

The two-dimensional analog of the high Reynolds number approximation (10) is then found to be

$$p(\mathbf{x}, t) \approx \frac{-\rho_0 x_j}{2\pi\sqrt{2c_0}|\mathbf{x}|^{3/2}}\frac{\partial}{\partial t}\int_{-\infty}^{t-|\mathbf{x}|/c_0} \frac{\mathrm{d}\tau}{\sqrt{t-\tau-|\mathbf{x}|/c_0}} \int (\boldsymbol{\omega} \wedge \mathbf{v}\cdot\nabla Y_j)(\mathbf{y}, \tau)\, \mathrm{d}y_1\, \mathrm{d}y_2, \quad |\mathbf{x}| \to \infty. \tag{12}$$

Solutions (10) and (12) are consistent with the corresponding approximations to Curle's [18] solution of the aerodynamic sound problem in three and two-dimensions:

$$p(\mathbf{x}, t) \approx \begin{cases} \dfrac{x_j}{4\pi c_0 |\mathbf{x}|^2} \dfrac{\partial F_j}{\partial t}\left(t - \dfrac{|\mathbf{x}|}{c_0}\right), & \text{three dimensions,} \\ \dfrac{x_j}{2\pi\sqrt{2c_0}\,|\mathbf{x}|^{3/2}} \dfrac{\partial_j}{\partial t} \displaystyle\int_{-\infty}^{t-|\mathbf{x}|/c_0} \dfrac{F_j(\tau)\,\mathrm{d}\tau}{\sqrt{t-\tau-|\mathbf{x}|/c_0}}, & \text{two dimensions,} \end{cases} \quad |\mathbf{x}| \to \infty, \quad (13)$$

where, respectively, $\mathbf{F}(t)$ is the net force exerted on the fluid in three-dimensions, and the force *per unit span* in two dimensions These formulae reduce to the corresponding equations (10) and (12) when the motion in the vicinity of the body can be regarded as incompressible, because the component $F_j$ of the force exerted on the fluid (per unit span in two dimensions) by a *stationary body in high Reynolds number flow* is given in terms of the vorticity by [4, 21]

$$F_j = -\rho_0 \int (\boldsymbol{\omega} \wedge \mathbf{v})(\mathbf{y}, t) \cdot \nabla Y_j(\mathbf{y})\,\mathrm{d}^n \mathbf{y}, \quad (14)$$

where $n = 2$ or 3 according to whether the geometry is two or three dimensional.

## 3. BLADE–VORTEX INTERACTIONS IN TWO DIMENSIONS

We consider both the *linear* and *non-linear* theories of the two-dimensional interaction of a rectilinear vortex with a strip airfoil. The motion is assumed to occur at high Reynolds number, so that viscosity can be ignored except possibly for its effect via the Kutta condition at the sharp trailing edge [14], and at sufficiently small Mach number that the motion in the neighborhood of the airfoil may be regarded as incompressible. The general problem is illustrated in Figure 2, which shows a vortex of circulation $\Gamma$ in motion in the neighborhood of a rigid airfoil of chord $2a$ occupying $-a < x_i < a$, $x_2 = 0$. Conditions are uniform in the $x_3$ direction (out of the plane of the paper in the figure), and there is no mean circulation about the airfoil. Consideration is given to cases with and without a mean flow in the $x_1$ direction.

### 3.1. EQUATION OF MOTION OF THE VORTEX

At time $t$ let the vortex be at $\mathbf{x} \equiv (x_1, x_2) = \mathbf{x}_0(t)$, so that $\boldsymbol{\omega} = \Gamma \mathbf{k} \delta(x_1 - x_{01}(t))\,\delta(x_2 - x_{02}(t))$, and the vortex translational velocity $\mathbf{v}_0 = \mathrm{d}\mathbf{x}_0/\mathrm{d}t$, where $\mathbf{k}$ is a unit vector out of the plane of the paper in Figure 2.

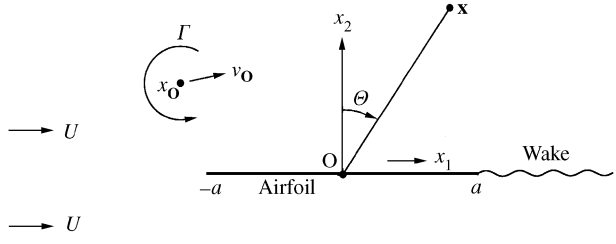


Figure 2. Interaction of a line vortex $\Gamma$ with a two-dimensional airfoil at zero mean angle of attack to a mean flow in the $x_1$ direction.

Define $z = x_1 + ix_2$, $z_0 = x_{01} + ix_{02}$. The transformation [22]

$$\zeta = \frac{z}{a} + \sqrt{\frac{z^2}{a^2} - 1}, \tag{15}$$

maps the fluid region in the $z$-plane of the airfoil into the region $|\zeta| > 1$ in the $\zeta$-plane. The "upper" and "lower" faces of the airfoil ($x_2 = \pm 0$), respectively, transform into the upper and lower halves ($\mathrm{Im}\,\zeta \gtrless 0$) of the unit circular cylinder $|\zeta| = 1$, and the vortex maps into an equal vortex at $\zeta = \zeta_0$, say.

In the absence of mean flow ($U = 0$) and when there is no mean circulation about the cylinder (and therefore about the airfoil), the complex potential $w(\zeta)$ of incompressible, inviscid motion in the $\zeta$-plane is obtained by placing an image vortex $-\Gamma$ within the cylinder at the *inverse point* $\zeta = 1/\zeta_0^*$ together with a vortex $+\Gamma$ at the center. These vortices ensure that the total circulation around the cylinder vanishes. Then

$$w(\zeta) = -\frac{i\Gamma}{2\pi}\ln(\zeta - \zeta_0) + \frac{i\Gamma}{2\pi}\ln\left(\zeta - \frac{1}{\zeta_0^*}\right) - \frac{i\Gamma}{2\pi}\ln\zeta.$$

The corresponding velocity potential in the $z$-plane is found by setting $\zeta = \zeta(z)$. Because a mean flow in the $x_1$ direction is unaffected by the airfoil, its contribution can be included by augmenting $w(z)$ by $Uz$. We then find

$$w(z) = -\frac{i\Gamma}{2\pi}\ln(\zeta(z) - \zeta(z_0)) + F(z), \tag{16}$$

where

$$F(z) = \frac{i\Gamma}{2\pi}\ln\left(\zeta(z) - \frac{1}{\zeta(z_0)^*}\right) - \frac{i\Gamma}{2\pi}\ln\zeta(z) + U_z.$$

The velocity potential $W(z)$ determining the motion of the free vortex at $z_0$ is obtained by subtracting the "self-potential" $-(i\Gamma/2\pi)\ln(z - z_0)$ from the right side of equation (16) [19, 22]. The complex velocity of the vortex is then equal to $W'(z_0)$ (where the prime denotes differentiation with respect to $z$ *after which* the substitution $z = z_0$ is made), with the explicit representation

$$\frac{dz_0^*}{dt} \equiv \frac{dx_{01}}{dt} - i\frac{dx_{02}}{dt} = W'(z_0) \equiv -\frac{i\Gamma\zeta''(z_0)}{4\pi\zeta'(z_0)} + F'(z_0),$$

i.e.,

$$\frac{dZ^*}{dt} = \frac{i\Gamma}{4\pi a\sqrt{Z^2 - 1}}\left\{\frac{Z}{\sqrt{Z^2 - 1}} - 1 + \frac{2}{|\zeta_0|^2 - 1}\right\} + U, \tag{17}$$

where

$$Z = \frac{z_0}{a}, \qquad \zeta_0 = Z + \sqrt{Z^2 - 1}.$$

Equation (17) takes no account of vortex shedding from the trailing edge, i.e., of the unsteady Kutta condition [14]. In the linearized approximation (where the image vortices are ignored, and the vortex is assumed to convect passively at the mean stream velocity $U$), this can be rectified by assuming the shed vorticity to lie within a thin vortex sheet

downstream of the trailing edge at $x_1 = a$ and to convect downstream at speed $U$ [15]. This would lead to the Sears representation of the sound produced by the vortex–airfoil interaction [4]. We shall not pursue this, however, because it limits the discussion to linearized motions.

### 3.2. THE ACOUSTIC PRESSURE

The farfield sound produced by the interaction is calculated using the two-dimensional formula (12), which has the explicit form

$$p(\mathbf{x}, t) \approx \frac{-\rho_0 \Gamma x_j}{2\pi\sqrt{2c_0|\mathbf{x}|^{3/2}}} \frac{\partial}{\partial t} \int_{-\infty}^{t-|\mathbf{x}|/c_0} \left\{ \frac{\mathrm{d}x_{01}}{\mathrm{d}\tau} \frac{\partial Y_j}{\partial y_2} - \frac{\mathrm{d}x_{02}}{\mathrm{d}\tau} \frac{\partial Y_j}{\partial y_1} \right\}_{\mathbf{x}_0(\tau)} \frac{\mathrm{d}\tau}{\sqrt{t-\tau-|\mathbf{x}|/c_0}}, \quad (18)$$

where the Kirchhoff vector for the strip airfoil has the components [4]

$$Y_1 = y_1, \qquad Y_2 = \mathrm{Re}(-\mathrm{i}\sqrt{z^2 - a^2}), \quad z = y_1 + \mathrm{i}y_2. \quad (19)$$

Let $\Theta$ denote the angle depicted in Figure 2 in the direction of an observer at $\mathbf{x}$ in the far field. Then equation (18) becomes

$$p(\mathbf{x}, t) \approx \frac{\rho_0 \Gamma \sin\Theta}{2\pi\sqrt{2c_0|\mathbf{x}|}} \frac{\partial}{\partial t} \int_{-\infty}^{t-|\mathbf{x}|/c_0} \frac{\mathrm{d}x_{02}}{\mathrm{d}\tau}(\tau) \frac{\mathrm{d}\tau}{\sqrt{t-\tau-|\mathbf{x}|/c_0}}$$
$$- \frac{\rho_0 \Gamma \cos\Theta}{2\pi\sqrt{}} 2c_0|\mathbf{x}| \frac{\partial}{\partial t} \int_{-\infty}^{t-|\mathbf{x}|/c_0} \left\{ \frac{\mathrm{d}x_{01}}{\mathrm{d}\tau} \frac{\partial Y_2}{\partial y_2} - \frac{\mathrm{d}x_{02}}{\mathrm{d}\tau} \frac{\partial Y_2}{\partial y_1} \right\}_{\mathbf{x}_0(\tau)} \frac{\mathrm{d}\tau}{\sqrt{t-\tau-|\mathbf{x}|/c_0}}.$$

The two integrals represent dipole acoustic fields. According to Curle's theory [18] and formula (14), the dipole strengths are determined by the unsteady force $(F_1, F_2)$ exerted on the fluid per unit span of the airfoil. The first is aligned with the airfoil chord (the mean flow direction) and represents the influence of *suction* forces at the leading and trailing edges [19]; the second component $F_2$ is equal and opposite to the unsteady lift produced by the interaction.

In general, the integrals must be evaluated numerically, using the solution of the equation of motion (17). Introduce the notation

$$\mathscr{W} = \frac{\mathrm{d}}{\mathrm{d}z}(-\mathrm{i}\sqrt{z^2 - a^2}) = \frac{-\mathrm{i}Z}{\sqrt{Z^2 - 1}}, \quad (20)$$

evaluated at the vortex $z = z_0$. Then

$$\left( \frac{\mathrm{d}x_{01}}{\mathrm{d}\tau} \frac{\partial Y_2}{\partial y_2} - \frac{\mathrm{d}x_{02}}{\mathrm{d}\tau} \frac{\partial Y_2}{\partial y_1} \right)_{\mathbf{x}_0(\tau)} \equiv -a\,\mathrm{Im}\left( \mathscr{W}(Z) \frac{\mathrm{d}Z}{\mathrm{d}\tau} \right), \qquad Z = \frac{z_0(\tau)}{a}$$

and the acoustic pressure becomes

$$p(\mathbf{x}, t) \approx \frac{\rho_0 \Gamma a}{2\pi\sqrt{2c_0|\mathbf{x}|}} \frac{\partial}{\partial t} \left\{ \sin\Theta \int_{-\infty}^{[t]} \mathrm{Im}\left( \frac{\mathrm{d}Z}{\mathrm{d}\tau} \right) \frac{\mathrm{d}\tau}{\sqrt{[t]-\tau}} + \cos\Theta \int_{-\infty}^{[t]} \mathrm{Im}\left( \mathscr{W}(Z) \frac{\mathrm{d}Z}{\mathrm{d}\tau} \right) \frac{\mathrm{d}\tau}{\sqrt{[t]-\tau}} \right\}, \quad (21)$$

where $[t] = t - |\mathbf{x}|/c_0$ is the retarded time.

Equations (17) and (21) determining the motion of the vortex motion and the acoustic pressure will now be applied to several different special cases.

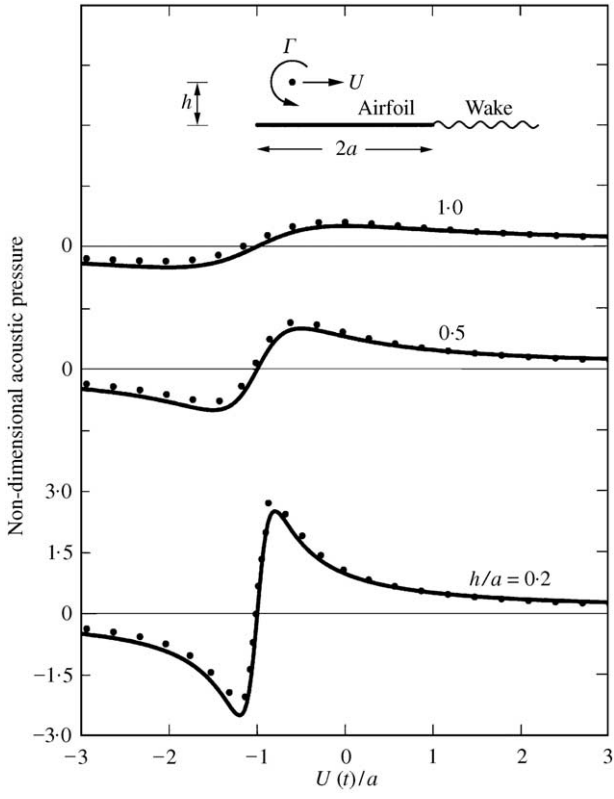


Figure 3. Comparison of approximate (▬▬) and exact (•••) linear theory acoustic pressure signatures produced by a two-dimensional vortex–airfoil interaction for different values of $h/a$.

### 3.3. LINEAR THEORY

According to linear theory, the vortex $\Gamma$ is swept past the airfoil along a trajectory parallel to the $x_1$ direction at precisely the uniform mean flow speed $U$. Only the second integral in equation (21) contributes to the sound (because $\mathrm{d}Z/\mathrm{d}\tau = U/a$ is real). This is the case illustrated in the upper part of Figure 3. When the standoff distance $h \ll a$, the characteristic scale of the dominant motions near the airfoil is small compared to the chord $2a$, and sound production occurs principally at the leading and trailing edges. Mathematically, the importance of the edges as sources of sound occurs because the Green function is singular at these points ($Z = \pm 1$) where $\mathscr{W}(Z)$ defined in equation (20) is unbounded. At high reduced frequencies, the main contribution to the second integral in equation (21) is then from the neighborhood of those retarded times where $|Z(\tau) \pm 1|$ is small.

But, at these high reduced frequencies vortex shedding causes the level of sound production at the trailing edge to be small [4] without affecting sound generation at the leading edge. We can formally account for this simply by *ignoring* the contribution to integral (21) from the neighborhood of the trailing edge. This is equivalent to expanding $\mathscr{W}(Z)$ about the leading edge $Z = -1$, i.e., to introducing the approximation

$$\mathscr{W}(Z) \approx \frac{1}{\sqrt{2}\sqrt{Z+1}}, \tag{22}$$

where the branch cut for $\sqrt{Z+1}$ runs along the real axis from $Z = -1$ to $+\infty$.

By making this substitution into equation (21), measuring time from the instant that the vortex crosses the midchord $x_1 = 0$ of the airfoil (so that $Z = U\tau/a + ih/a$), and making the change of integration variable $\xi = 1/\sqrt{t - \tau - |\mathbf{x}|/c_0}$, the second integral in equation (21) can be evaluated explicitly to yield the lift dipole acoustic pressure in the form

$$\frac{p(\mathbf{x}, t)}{\rho_0 \Gamma U \sqrt{M} \cos\Theta (a/|\mathbf{x}|)^{1/2}/4\pi a} \approx \frac{(U[t]/a + 1)}{(U[t]/a + 1)^2 + (h/a)^2}, \quad |\mathbf{x}| \to \infty, \tag{23}$$

where $M = U/c_0$.

The non-dimensional acoustic pressure signature determined by this formula (i.e., the right of equation (23)) is plotted as the solid curves in Figure 3 for $h/a = 0{\cdot}2$, $0{\cdot}5$, $1{\cdot}0$.

To assess the utility of approximation (22) in taking proper account of vortex shedding, a comparison can be made with predictions derived from the Sears, linear theory calculation of the unsteady life force per unit span $-F_2(\tau)$, say, which takes full account of the Kutta condition [15]. The sound is then found from the second of equations (13) (where $j = 2$) in the present linear theory) in the form

$$\frac{p(\mathbf{x}, t)}{\rho_0 \Gamma U \sqrt{M} \cos\Theta (a/|\mathbf{x}|)^{1/2}/4\pi a} \approx \sqrt{2\pi}\,\mathrm{Re} \int_0^\infty (i\lambda)^{1/2}\, \mathscr{S}(\lambda) e^{-\lambda\{h/a + iU[t]/a\}}\, d\lambda, \quad |\mathbf{x}| \to \infty \tag{24}$$

where

$$\mathscr{S}(x) = \frac{2}{\pi x [H_0^{(1)}(x) + iH_1^{(1)}(x)]}$$

is the Sears function [4, 15] ($H_{0,1}^{(1)}(x)$ being Hankel functions). The corresponding acoustic pressure signatures are plotted as the dotted curves in Figure 3. The agreement with the approximate theory is remarkably good even when $h/a$ is as large as unity, when the characteristic frequency of the unsteady motion is small, and might be expected to lie outside the range where the "high-frequency" approximation (22) is applicable. Note that the predicted pressure profiles are consistent with expectations: before the vortex reaches the leading edge it induces an upwash creating a positive *lift* on the airfoil; the lift becomes negative when the vortex is downstream of the edge. The dipole source strength is equal and opposite to this force, so that the pressure radiated directly above the airfoil is initially negative and then becomes positive, in qualitative agreement with equation (13).

### 3.4. NON-LINEAR THEORY

When account is taken of "image vortices" in the airfoil, the trajectory of the vortex in the neighborhood of the airfoil is no longer parallel to the mean flow direction, and must be determined by numerical integration of equation (17). To do this introduce a dimensionless velocity ratio $\varepsilon$ and time $T$ defined by

$$\varepsilon = \frac{\Gamma}{4\pi a U}, \qquad T = \frac{Ut}{a},$$

in terms of which equation (17) becomes

$$\frac{dZ^*}{dT} = \frac{i\varepsilon}{\sqrt{Z^2 - 1}} \left\{ \frac{Z}{\sqrt{Z^2 - 1}} - 1 + \frac{2}{|\zeta_0|^2 - 1} \right\} + 1, \tag{25}$$

which is suitable for numerical integration.

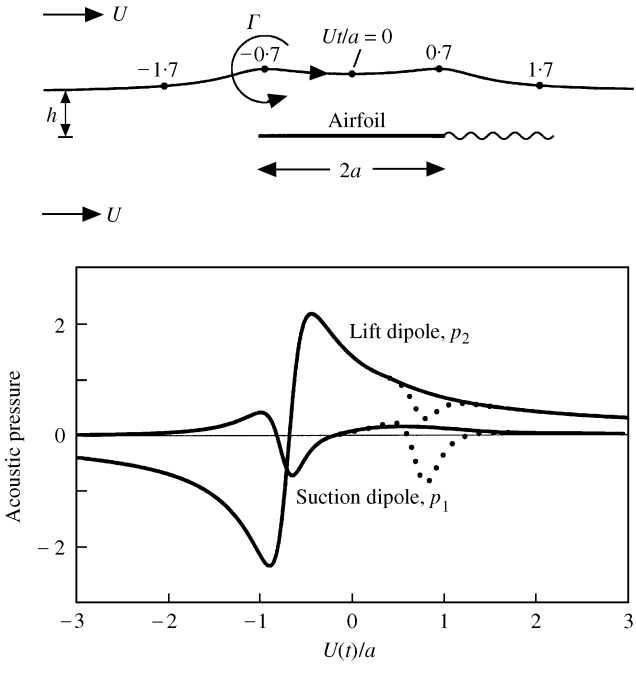


Figure 4. Non-linear interaction of a line vortex with a two-dimensional airfoil for $h/a = 0{\cdot}2$, $\varepsilon = \Gamma/4\pi aU = 0{\cdot}2$. The small trailing edge generated acoustic "blips" (•••) are removed by interpolating between the predicted acoustic pressures (27) on either side of the blips.

If the initial standoff distance at $x_1 = -\infty$ is $h$, the integration is started at a large distance $L$ upstream of the airfoil midchord, at say $L = 20a$, by prescribing the initial position of the vortex to be $Z = -L/a + \mathrm{i}h/a$. The upper part of Figure 4 shows the trajectory calculated in this way for $\varepsilon = 0{\cdot}2$, $h/a = 0{\cdot}2$, where the time is measured from the instant that the vortex passes the midchord of the airfoil. The non-linear influence of the image vorticity is to shift the initially rectilinear trajectory of the vortex away from the airfoil in the direction of the "vortex force" $\boldsymbol{\omega} \wedge \mathbf{U}$ ($\mathbf{U} = U\mathbf{i}$). The vortex is closest to the airfoil at $Ut/a = 0$, where $x_{02} \sim 0{\cdot}28a$, and where convection by the images increases the translation speed of the vortex from $U$ to approximately $1{\cdot}71U$.

The sound generated as the vortex passes the airfoil is given by equation (21). Vortex shedding from the trailing edge is modelled by using approximation (22) for $\mathscr{W}(Z)$. The integrals are evaluated numerically in terms of a dimensionless vortex convection velocity.

$$\frac{\mathrm{d}Z}{\mathrm{d}\hat{T}} = u(\hat{T}) + \mathrm{i}v(\hat{T}), \quad \text{where} \quad \hat{T} = \frac{U\tau}{a}.$$

Then, setting $M = U/c_0$,

$$\frac{p(\mathbf{x}, t)}{\rho_0 \Gamma U \sqrt{M}\,(a/|\mathbf{x}|)^{1/2}/4\pi a}$$

$$\approx 2^{1/2} \frac{\mathrm{d}}{\mathrm{d}T} \left\{ \sin\Theta \int_{-\infty}^{[T]} \frac{v(\hat{T})\,\mathrm{d}\hat{T}}{\sqrt{[T] - \hat{T}}} + \cos\Theta \int_{-\infty}^{[T]} \frac{\mathrm{Im}(\mathscr{W}(Z)(u + \mathrm{i}v))(\hat{T})\,\mathrm{d}\hat{T}}{\sqrt{[T] - \hat{T}}} \right\}$$

$$= 2^{3/2} \sin \Theta \frac{\mathrm{d}}{\mathrm{d}T} \int_0^\infty v([T] - \lambda^2)\, \mathrm{d}\lambda + 2^{3/2} \cos \Theta \frac{\mathrm{d}}{\mathrm{d}T} \int_0^\infty \mathrm{Im}(\mathscr{W}(Z)(u + \mathrm{i}v))([T] - \lambda^2))\, \mathrm{d}\lambda$$

$$\approx \frac{p_1(\mathbf{x}, t)}{\rho_0 \Gamma U \sqrt{M}\, (a/|\mathbf{x}|)^{1/2}/4\pi a} + \frac{p_2(\mathbf{x}, t)}{\rho_0 \Gamma U \sqrt{M}\, (a/|\mathbf{x}|)^{1/2}/4\pi a}, \tag{26}$$

where $T = Ut/a$, $[T] = U[t]/a$, and the integration variable $\hat{T}$ has been replaced by $\lambda = \sqrt{[T] - \hat{T}}$. The final integrals are easily evaluated numerically when the path of the vortex has been determined. The upper limit of integration is actually finite, because the source terms vanish as soon as $[T] - \lambda^2$ reduces to the non-dimensional time at which the computation of the vortex path begins (where the vortex is sufficiently far upstream such that it effectively produces no sound by interaction with the airfoil).

The components $p_1(\mathbf{x}, t)$, $p_2(\mathbf{x}, t)$ defined by equation (26) correspond, respectively, to the dipole sound produced by the unsteady suction and lift forces; their non-dimensional forms

$$\frac{p_1(\mathbf{x}, t)}{\rho_0 \Gamma U \sqrt{M} \sin \Theta (a/|\mathbf{x}|)^{1/2}/4\pi a} \quad \text{and} \quad \frac{p_2(\mathbf{x}, t)}{\rho_0 \Gamma U \sqrt{M} \cos \Theta (a/|\mathbf{x}|)^{1/2}/4\pi a} \tag{27}$$

are plotted in Figure 4. Vortex shedding must smooth out the profiles of the pressure signatures at the retarded times when the vortex is close to the trailing edge.But the calculated pressures exhibit "blips" shown dotted in the figure. These arise because, although the numerical calculation has accounted for vortex shedding in evaluating the dipole source strengths, the effect of shedding was not included in the calculation of the vortex *trajectory*. However, the smoothing influence of shedding at a sharp edge acts to remove the blips, and the pressure signatures actually have profiles similar to those depicted by the solid curves in the figure, obtained by interpolating between the calculated pressures on either side of the blips (by joining smoothly the monotonically decreasing sections of the profiles on either side of the blips). The overall lift dipole radiation is then very similar to the linear theory prediction of Figure 3 for $h/a = 0{\cdot}2$ (and agrees well with a recent numerical modelling of this problem by Wood [23]), but there is no linear theory counterpart of the suction dipole sound.

An interesting special case occurs when the initial standoff distance of the vortex $h = 0$ (Figure 5). In the linearized approximation, the vortex would strike the leading edge of the airfoil at $U[t]/a = -1$, at which time the linear theory acoustic pressure (23) becomes infinite. This singular events does not occur because the vortex trajectory is deflected by the image vorticity (in the direction of $\boldsymbol{\omega} \wedge \mathbf{U}$) to pass around the airfoil. The upper part of Figure 5 illustrates this for the same value of the velocity ratio $\varepsilon = \Gamma/4\pi aU = 0{\cdot}2$ considered above. The maximum convection velocity of the vortex (at $Ut/a = 0$) is now $\sim 2{\cdot}3U$, over twice the mean stream velocity, and the effective frequency of the sound is greatly increased. The corresponding suction- and lift-dipole acoustic pressures $p_1$ and $p_2$ shown in the figure are also much larger.

### 3.5. PERIODIC VORTEX MOTION

When there is no mean flow past the airfoil ($U = 0$), the characteristic velocity and dimensionless time are

$$\mathscr{W} = \frac{\Gamma}{4\pi a}, \qquad T = \frac{\mathscr{W} t}{a}$$

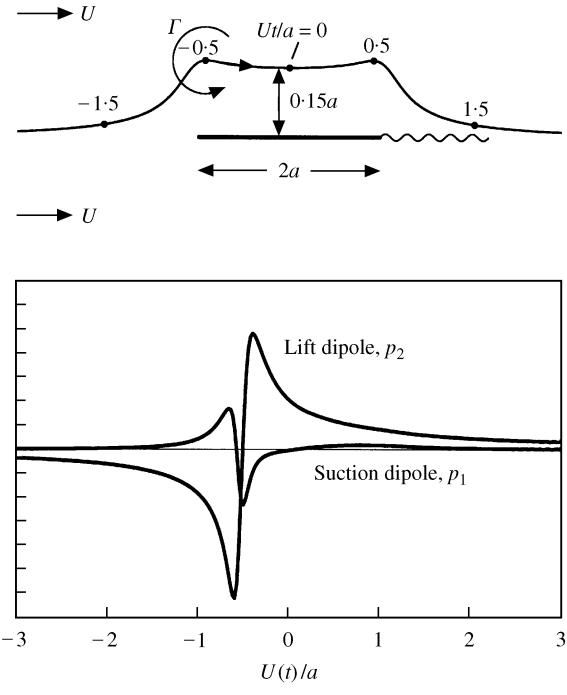


Figure 5. Non-linear interaction of a line vortex with a two-dimensional airfoil for $h/a = 0$, $\varepsilon = \Gamma/4\pi aU = 0{\cdot}2$. Small trailing edge generated acoustic "blips" have been removed by interpolating between the predicted acoustic pressures (27) on either side of the blips.

and the equation of motion (17) of the vortex reduces to

$$\frac{\mathrm{d}Z^*}{\mathrm{d}T} = \frac{\mathrm{i}}{\sqrt{Z^2-1}}\left\{\frac{Z}{\sqrt{Z^2-1}} - 1 + \frac{2}{|\zeta_0|^2-1}\right\}.$$

The solutions are periodic orbits *around* the airfoil. That shown in the upper-half of Figure 6 is for a vortex with $\Gamma > 0$ released at 0 where $x_{01} = -2a$, $x_{02} = 0$. The calculated period is $T_0 = \mathscr{V}t_0/a \approx 35{\cdot}84$.

Although an orbiting vortex motion of this kind cannot be realized in practice (because of both diffusion of the concentrated vortex core and the continual shedding of additional vorticity from the edges of the airfoil), it is nonetheless instructive to calculate the accompanying radiation. By writing

$$\hat{T} = \frac{\mathscr{V}\tau}{a} \quad \text{and} \quad \frac{\mathrm{d}Z}{\mathrm{d}\hat{T}} = u(\hat{T}) + \mathrm{i}v(\hat{T})$$

in the general formula (21) for the acoustic pressure, the non-dimensional suction and lift acoustic pressures are found to be given by the following modified form of equation (26):

$$\frac{p_1(\mathbf{x},t)}{\rho_0\mathscr{V}^2\sqrt{M}\,(a/|\mathbf{x}|)^{1/2}} + \frac{p_2(\mathbf{x},t)}{\rho_0\mathscr{V}^2\sqrt{M}\,(a/|\mathbf{x}|)^{1/2}}$$
$$\approx 2^{1/2}\frac{\mathrm{d}}{\mathrm{d}T}\left\{\sin\Theta\int_{-\infty}^{[T]}\frac{v(\hat{T})\,\mathrm{d}\hat{T}}{\sqrt{[T]-\hat{T}}} + \cos\Theta\int_{-\infty}^{[T]}\frac{\mathrm{Im}\,(\mathscr{W}(Z)(u+\mathrm{i}v))(\hat{T})\,\mathrm{d}\hat{T}}{\sqrt{[T]-\hat{T}}}\right\}, \tag{28}$$

where $M = \mathscr{V}/c_0$, and $\mathscr{W}(Z)$ is given by equation (20) in the absence of vortex shedding.

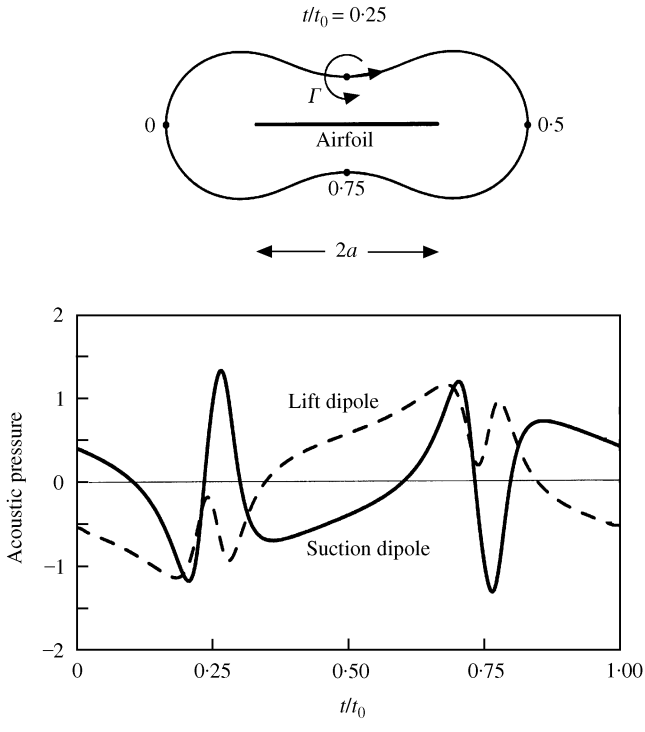


Figure 6. Sound produced by two-dimensional periodic motion of a vortex around the airfoil in the absence of mean flow. The vortex was initially released at the point 0 where $x_1 = -2a$, $x_2 = 0$, and circumnavigates the airfoil in time $Vt_0/a \approx 35{\cdot}84$.

It follows by inspection and from the numerical solution, that when $T$ is measured as indicated in Figure 6, from the point of release at $Z = -2$, the suction and dipole source strengths have period $T_0$, and possess Fourier expansions of the form

$$v(T) = \sum_{n=1}^{\infty} a_n \cos\left(\frac{2\pi nT}{T_0}\right), \qquad \mathrm{Im}\,(\mathscr{W}(Z)(u + \mathrm{i}v))\,(T) = \sum_{n=1}^{\infty} b_n \sin\left(\frac{2\pi nT}{T_0}\right),$$

where the coefficients $a_n$, $b_n$ can be calculated by using the numerical solution for the orbit to evaluate

$$a_n = \frac{2}{T_0}\int_0^{T_0} v(T)\cos\left(\frac{2\pi nT}{T_0}\right)\mathrm{d}T, \qquad b_n = \frac{2}{T_0}\int_0^{T_0} \mathrm{Im}\,(\mathscr{W}(Z)(u + \mathrm{i}v))(T)\sin\left(\frac{2\pi nT}{T_0}\right)\mathrm{d}T.$$

By making the change of integration variable $\lambda = \sqrt{[T] - \hat{T}}/\sqrt{T_0}$, the right side of equation (28) now becomes

$$\frac{4\sqrt{2}\pi}{\sqrt{T_0}}\sum_{n=0}^{\infty}\left\{-a_n n\sin\Theta\int_0^{\infty}\sin\left[2\pi n\left(\frac{[T]}{T_0}-\lambda^2\right)\right]\mathrm{d}\lambda\right.$$

$$\left. + b_n n\cos\Theta\int_0^{\infty}\cos\left[2\pi n\left(\frac{[T]}{T_0}-\lambda^2\right)\right]\mathrm{d}\lambda\right\}.$$

Hence, the suction and lift force dipole fields are given, respectively, by

$$\frac{p_1(\mathbf{x}, t)}{\rho_0 \mathscr{V}^2 \sqrt{M} \sin \Theta (a/|\mathbf{x}|)^{1/2}} \approx -\frac{2\pi}{\sqrt{T_0}} \sum_{n=1}^{\infty} a_n \sqrt{n} \sin\left[\frac{2n\pi t}{t_0} - \frac{\pi}{4}\right],$$

$$\frac{p_2(\mathbf{x}, t)}{\rho_0 \mathscr{V}^2 \sqrt{M} \cos \Theta (a/|\mathbf{x}|)^{1/2}} \approx \frac{2\pi}{\sqrt{T_0}} \sum_{n=1}^{\infty} b_n \sqrt{n} \cos\left[\frac{2n\pi t}{t_0} - \frac{\pi}{4}\right], \quad |\mathbf{x}| \to \infty,$$

where [ ] denotes evaluation at the retarded time $t - |\mathbf{x}|/c_0$. The corresponding non-dimensional pressures are plotted in Figure 6 (taking 26 terms in each series); both have similar orders of magnitude, and exhibit rapid variations when the vortex is above and below the airfoil (because of the phase lag $\pi/4$ associated with two-dimensional propagation).

## 4. PARALLEL BLADE–VORTEX INTERACTIONS IN THREE DIMENSIONS

We now examine to what extent the simple two-dimensional methods of the previous section can be adapted to wings of finite span and variable, but acoustically compact chord for problems of the kind shown in Figure 7. The general representation of the sound for an airfoil of arbitrary span can be found using the compact Green function (6) [4], but we shall consider only the case where the span is also compact; predictions for non-compact span will be intermediate between those for the compact-span case and the results of section 3.

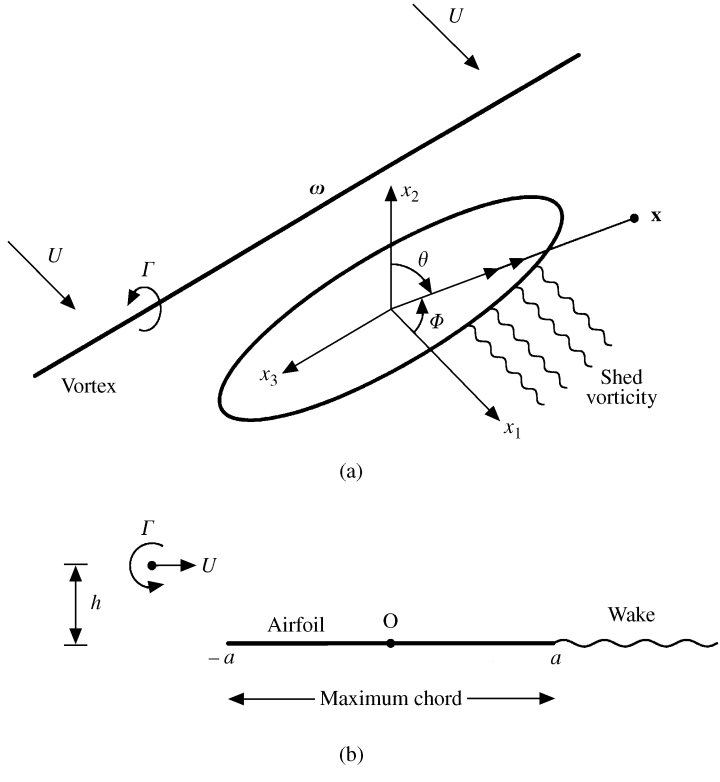


Figure 7. (a) Parallel blade–vortex interaction for an airfoil of finite span. (b) Side view in the linearized approximation, when the convection velocity equals the mean stream velocity $U$.

Consider a planar airfoil of either rectangular or elliptic planform, orientated as illustrated in Figure 7(a) at zero angle of attack to a mean flow at speed $U$ in the $x_1$ direction. A spanwise line vortex of strength $\Gamma$ is swept past the airfoil at an initial standoff distance $h$ above the airfoil, as indicated in the side view of Figure 7(b). The section of the line vortex that interacts with the airfoil is assumed to remain rectilinear during the interaction, with representation

$$\boldsymbol{\omega} = \Gamma \mathbf{k} \delta(x_1 - x_{01}(t))\, \delta(x_2 - x_{02}(t)),$$

where $\mathbf{x}_0 = (x_{01}, x_{02}, 0)$ is the vortex position at time $t$ and $\mathbf{k}$ is a unit vector in the $x_3$ direction.

When the airfoil is compact the acoustic pressure is given by equation (10). For an airfoil of span $L$ (between $-\frac{1}{2}L < x_3 < \frac{1}{2}L$), the Kirchhoff vector can be approximated by [4]

$$Y_1 = y_1, \qquad Y_2 = \begin{cases} \mathrm{Re}(-\mathrm{i}\sqrt{z^2 - \hat{a}(y_3)^2}), & |y_3| < \frac{1}{2}L, \\ y_2, & |y_3| > \frac{1}{2}L, \end{cases} \qquad Y_3 = y_3, \quad z = y_1 + \mathrm{i}y_2,$$

where $2\hat{a}(y_3)$ is the airfoil chord at the spanwise location $y_3$. For a rectangular planform $\hat{a}(y_3) \equiv a =$ constant; for an elliptic planform $\hat{a}(y_3)$ takes a maximum value of $a$ at $y_3 = 0$, and we shall write

$$\frac{\hat{a}(y_3)}{a} = \sqrt{1 - \frac{4y_3^2}{L^2}}, \qquad |y_3| < \tfrac{1}{2}L. \tag{29}$$

Vorticity is shed into the wake of the airfoil in accordance with the Kutta condition. This smoothes out conditions at the trailing edge, so that sound is generated primarily by interaction of the vortex with the leading edge. The Kutta condition will be applied (as in section 3) by formally removing the trailing edge singularity of the Green function, i.e., by modifying the $x_2$-component of $\mathbf{Y}$ as follows:

$$Y_2 = \mathrm{Re}(\sqrt{2\hat{a}(y_3)}\,\sqrt{z + \hat{a}(y_3)}), \qquad |y_3| < \tfrac{1}{2}L.$$

Then, neglecting relatively small end-effects, at the airfoil tips, equation (10) supplies

$$\begin{aligned} p(\mathbf{x}, t) &\equiv p_1(\mathbf{x}, t) + p_2(\mathbf{x}, t) \\ &\approx \frac{\rho_0 \Gamma \cos\Phi}{4\pi c_0 |\mathbf{x}|} \frac{\partial}{\partial t} \int_{-L/2}^{L/2} \left[ \frac{\mathrm{d}x_{02}}{\mathrm{d}t} \right] \mathrm{d}y_3 \\ &\quad + \frac{\rho_0 \Gamma \cos\Theta}{4\sqrt{2}\pi c_0 |\mathbf{x}|} \frac{\partial}{\partial t} \int_{-L/2}^{L/2} \left[ \mathrm{Im}\left( \frac{\mathrm{d}z_0}{\mathrm{d}t} \frac{\sqrt{\hat{a}(y_3)}}{\sqrt{z_0(t) + \hat{a}(y_3)}} \right) \right] \mathrm{d}y_3, \quad |\mathbf{x}| \to \infty, \end{aligned} \tag{30}$$

where $\Phi$, $\Theta$ are, respectively, the angles shown in Figure 7(a) between the $x_1$- and $x_2$-axis and the radiation direction to the observer at $\mathbf{x}$, $z_0(t) = x_{01}(t) + \mathrm{i}x_{02}(t)$, and quantities in square braces are evaluated at the retarded time $[t] = t - |\mathbf{x}|/c_0$.

The first term on the right is the suction force dipole, aligned with the airfoil chord. The dipole strength depends on the $x_2$-component of the vortex convection velocity, and is non-zero only when account is taken of non-linear interactions between the airfoil and vortex. The second term in equation (30) is the conventional lift dipole radiation.

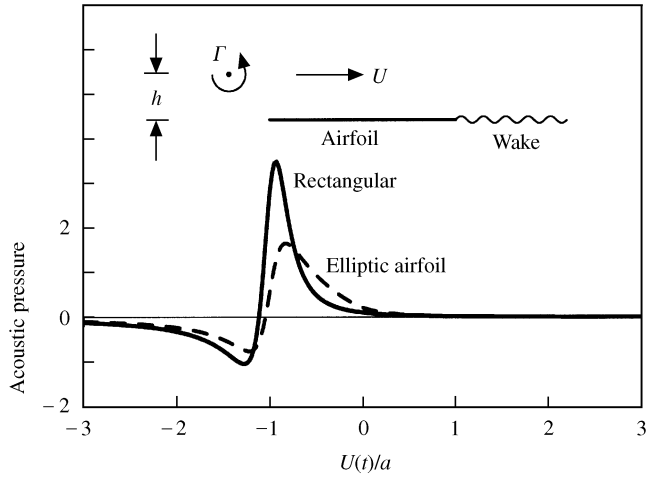


Figure 8. Linear theory prediction (31) of sound produced by parallel blade–vortex interactions for rectangular (——) and elliptic (- - -) airfoils for $h/a = 0{\cdot}2$.

### 4.1. LINEAR THEORY

When the back-reaction of the airfoil on the vortex is ignored, the convection velocity of the vortex is equal to the mean stream velocity, so that

$$\frac{\mathrm{d}x_{01}}{\mathrm{d}t} = U, \quad \frac{\mathrm{d}x_{02}}{\mathrm{d}t} = 0.$$

The radiation is produced entirely by the lift dipole, and if the vortex is assumed to cross the midchord of the airfoil at time $t = 0$, equation (30) reduces to

$$\frac{p_2(\mathbf{x}, t)}{\rho_0 \Gamma U M \cos\Theta (L/|\mathbf{x}|)/4\pi a} \approx -\frac{1}{2^{3/2}} \int_{-1/2}^{1/2} \mathrm{Im}\left( \frac{\sqrt{\hat{a}/a}}{(U[t]/a + \hat{a}/a + \mathrm{i}\, h/a)^{3/2}} \right) \mathrm{d}\hat{y}_3, \quad (31)$$

where $M = U/c_0$, $\hat{y}_3 = y_3/L$ and $\hat{a}/a$ is given by equation (29). For the rectangular planform ($\hat{a} \equiv a$) the right side of this formula evaluates to

$$-\frac{1}{2^{3/2}} \mathrm{Im}\left( \frac{1}{(U[t]/a + 1 + \mathrm{i}\, h/a)^{3/2}} \right),$$

which does not depend on the span $L$. The integral in equation (31) must be evaluated numerically for the elliptic planform.

The acoustic pressure signatures (left side of equation (31)) for rectangular and elliptic airfoils are plotted in Figure 8 for a vortex standoff distance $h/a = 0{\cdot}2$. The profiles are qualitatively similar to corresponding plot in Figure 3 for the two-dimensional interaction, except that in three dimensions the amplitude decreases much more rapidly with increasing retarded distance of the vortex from the leading edge. For the rectangular planform, the maximum amplitude is larger and the width of the acoustic pulse is narrower than for the elliptic planform; in the latter case, the peak interaction of the leading edge singularity (of the Green function) with the vortex occurs at different retarded times for different parts of the vortex, reducing the overall magnitude of the pressure and extending the interaction over a longer time period.

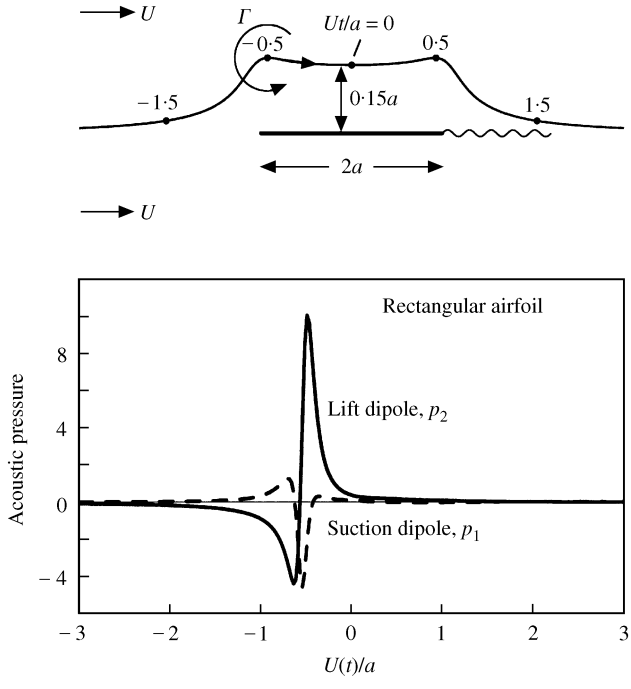


Figure 9. Non-linear interaction of a line vortex with a rectangular airfoil for $h/a = 0, \varepsilon = \Gamma/4\pi aU = 0{\cdot}2$. Small trailing edge generated acoustic "blips" have been removed by interpolating between the predicted acoustic pressures (32) on either side of the blips.

### 4.2. NON-LINEAR THEORY

When $h = 0$, the induced velocity field of image vorticity in the airfoil prevents a direct collision between the vortex and the airfoil by deflecting the trajectory to pass above the airfoil (for $\Gamma > 0$). This can be modelled in the case of the rectangular airfoil by assuming that the section of the vortex within the span $-\frac{1}{2}L < x_3 < \frac{1}{2}L$ follows a deflected path that is locally identical with that considered in section 3.4 for the two-dimensional problem, and by neglecting small contributions from the ends of the airfoil.

Introduce the notation

$$\varepsilon = \frac{\Gamma}{4\pi aU}, \qquad T = \frac{Ut}{a}, \qquad Z = \frac{z_0}{a}, \qquad \frac{\mathrm{d}Z}{\mathrm{d}T} = u(T) + \mathrm{i}v(T), \qquad \mathscr{W}(Z) = \frac{1}{\sqrt{2}\sqrt{Z+1}}.$$

Then equation (25) determines the motion of the vortex section within the span of the airfoil ($-\frac{1}{2}L < x_3 < \frac{1}{2}L$, where $\zeta_0$ is defined in terms of $z_0$ as in equation (15)), and the suction and lift dipole pressures are given by

$$\frac{p_1(\mathbf{x}, t)}{\rho_0 \Gamma U M \cos\Phi(L/|\mathbf{x}|)/4\pi a} \approx \left[\frac{dv}{\mathrm{d}T}\right],$$

$$\frac{p_2(\mathbf{x}, t)}{\rho_0 \Gamma U M \cos\Theta(L/|\mathbf{x}|)/4\pi a} \approx \frac{\partial}{\mathrm{d}T}\left[\mathrm{Im}\left(\mathscr{W}(Z)(u + \mathrm{i}v)\right)\right], \quad |\mathbf{x}| \to \infty, \tag{32}$$

where [ ] denotes evaluation at the retarded time $t - |\mathbf{x}|/c_0$.

These non-dimensional pressures are plotted in Figure 9 for a velocity ratio $\varepsilon = 0{\cdot}2$ when the vortex is released upstream with a standoff distance $h = 0$. The upper part of the figure

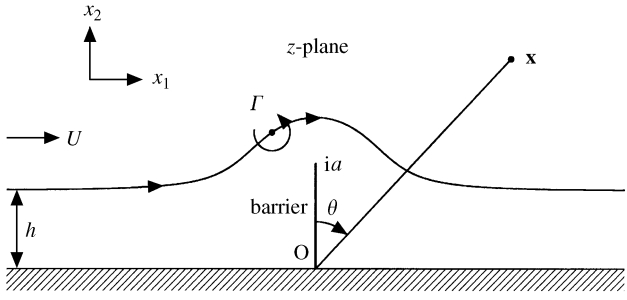


Figure 10. Sound production during the passage of a line vortex over a thin-wall barrier.

shows the path followed by those sections of the vortex inboard of the airfoil tips; it is the same as that in Figure 5 for the two-dimensional problem. Small and spurious acoustic pulses generated as the vortex passes the trailing edge (because its path is not predicted correctly there) have been removed from the pressure signatures (as in Figures 4 and 5). Three dimensionality is seen to produce leading edge generated acoustic pulses that are considerably narrower than those predicted in two dimensions.

## 5. VORTEX INTERACTING WITH A WALL BARRIER

The sound produced when vorticity interacts at low Mach number with surface irregularities on a nominally plane, rigid wall is attributable to dipole sources orientated parallel to the wall, i.e., to the unsteady *wall drag*. Kasoev [24] has given a very approximate analysis of a canonical problem of this type, in which a line vortex translates by self-induction over the vertical, thin projecting barrier illustrated in Figure 10. Let the wall coincide with the plane $x_2 = 0$ and the barrier extend along the $x_2$-axis from $x_2 = 0$ to $a > 0$. The vortex

$$\boldsymbol{\omega} = \Gamma \mathbf{k} \delta(x_1 - x_{01}(t)) \delta(x_2 - x_{02}(t))$$

is parallel to the barrier, and convects over the barrier in an irrotational mean stream that has uniform speed $U$ in the $x_1$ direction far from the barrier.

Define $z = x_1 + \mathrm{i}x_2$, $z_0 = x_{01} + \mathrm{i}x_{02}$. The transformation [22]

$$\zeta = \sqrt{\frac{z^2}{a^2} + 1} \tag{33}$$

maps the fluid region above the wall onto the upper-half $\mathrm{Im}\,\zeta > 0$ of the $\zeta$-plane. The "left" and "right" faces of the barrier ($x_1 = \mp 0$), respectively, transform into the intervals $-1 < \zeta < 0$ and $0 < \zeta < 1$ of the real $\zeta$-axis, and the vortex maps into an equal vortex at $\zeta = \zeta_0$. The method described in section 3.1 accordingly leads to the following equation of motion of the vortex:

$$\frac{\mathrm{d}Z^*}{\mathrm{d}T} = -\mathrm{i}\left\{\frac{1}{Z(Z^2+1)} - \frac{2Z}{Z^2 + 1 - |Z^2+1|}\right\} + \frac{\varepsilon Z}{\sqrt{Z^2+1}}, \tag{34}$$

where

$$Z = z_0/a, \quad T = Vt/a, \quad V = \Gamma/(4\pi a), \quad \varepsilon = U/V.$$

The last term on the right side of equation (34) represents the convection by the mean flow.

The two-dimensional compact Green function for this problem (applicable when the sound produced by the interaction has wavelength $\gg a$) must take account of the presence of the rigid wall at $x_2 = 0$, and is given by the following modification of equation (1) (see reference [4]):

$$G(\mathbf{x}, \mathbf{y}, t-\tau) \approx \frac{x_1 Y_1}{\pi\sqrt{2c_0}\,|\mathbf{x}|^{3/2}} \frac{\partial}{\partial t}\left\{\frac{\mathrm{H}(t-\tau-|\mathbf{x}|/c_0}{\sqrt{t-\tau-|\mathbf{x}|/c_0}}\right\}, \quad |\mathbf{x}| \to \infty, \tag{35}$$

where the Kirchhoff vector

$$Y_1 = \mathrm{Re}(\sqrt{z^2 + a^2}), \qquad z = y_1 + \mathrm{i}y_2, \tag{36}$$

which is the velocity potential of incompressible flow at right angles to the barrier in a direction parallel to the wall. $G$ represents the field of a dipole orientated parallel to the wall and perpendicular to the barrier, and the effect of the wall is to generate an equal 'image' dipole that just *doubles* the magnitude of the sound relative to the corresponding dipole in equation (11) in the absence of the wall.

The analog of equation (18) for the farfield acoustic pressure is therefore

$$p(\mathbf{x}, t) \approx \frac{-\rho_0 \Gamma x_1}{\pi\sqrt{2c_0}|\mathbf{x}|^{3/2}} \frac{\partial}{\partial t} \int_{-\infty}^{t-|\mathbf{x}|/c_0} \left\{\frac{\mathrm{d}x_{01}}{\mathrm{d}\tau}\frac{\partial Y_1}{\partial y_2} - \frac{\mathrm{d}x_{02}}{\mathrm{d}\tau}\frac{\partial Y_1}{\partial y_1}\right\}_{\mathbf{x}_0(\tau)} \frac{\mathrm{d}\tau}{\sqrt{t-\tau-|\mathbf{x}|/c_0}}. \tag{37}$$

According to equations (13) and (14), this is just the dipole sound generated by the unsteady drag force $F_1$ exerted on the fluid by the barrier, where (per unit span of the barrier)

$$F_1 = -\rho_0 \int \boldsymbol{\omega} \wedge \mathbf{v} \cdot \nabla Y_1 \,\mathrm{d}y_1 \,\mathrm{d}y_2 = -\rho_0 \Gamma \mathbf{k} \wedge \frac{\mathrm{d}\mathbf{x}_0}{\mathrm{d}t} \cdot \nabla Y_1(\mathbf{x}_0).$$

This implies that a *linear theory* of the vortex–barrier interaction (in which the vortex is convected at undisturbed, irrotational velocity of the mean stream) would predict that no dipole sound is generated as the vortex passes around the barrier, because in that case

$$\frac{\mathrm{d}\mathbf{x}_0}{\mathrm{d}t} = U\nabla Y_1(\mathbf{x}_0) \quad \text{and} \quad \mathbf{k} \wedge \nabla Y_1 \cdot \nabla Y_1 \equiv 0.$$

Following the procedure described in section 3, introduce the notations

$$\frac{\mathrm{d}Z}{\mathrm{d}T} = u(T) + \mathrm{i}v(T), \qquad \mathscr{W} = \frac{\mathrm{d}}{\mathrm{d}z}(\sqrt{z^2 + a^2}) = \frac{Z}{\sqrt{Z^2 + 1}} \tag{38}$$

evaluated at the vortex. Then equation (37) for the acoustic pressure can be cast in the form

$$\frac{p(\mathbf{x}, t)}{\rho_0 V^2 \sqrt{M \sin\Theta}(a/|\mathbf{x}|)^{1/2}} \approx 2^{5/2} \frac{\partial}{\partial T} \int_0^\infty \mathrm{Im}(\mathscr{W}(Z)(u + \mathrm{i}v))([T] - \lambda^2)\,\mathrm{d}\lambda, \tag{39}$$

where $[T] = V[t]/a$ is the non-dimensional retarded time, and $M = V/c_0$.

The vortex path equation (34) and the acoustic pressure integral (39) must be evaluated numerically, taking the initial position of the vortex several barrier heights $a$ upstream where its motion is unaffected by the presence of the barrier. The upper part of Figure 11 shows the vortex trajectories when the initial standoff distance of the vortex from the wall $h = 0{\cdot}75a$ for the two cases (1) of no mean flow, $U = 0$, and (2) $U = V$; the corresponding non-dimensional acoustic pressures (39) are plotted in the lower part of the figure. The effect of mean flow is to draw the trajectory marginally closer to the barrier as it passes the tip of

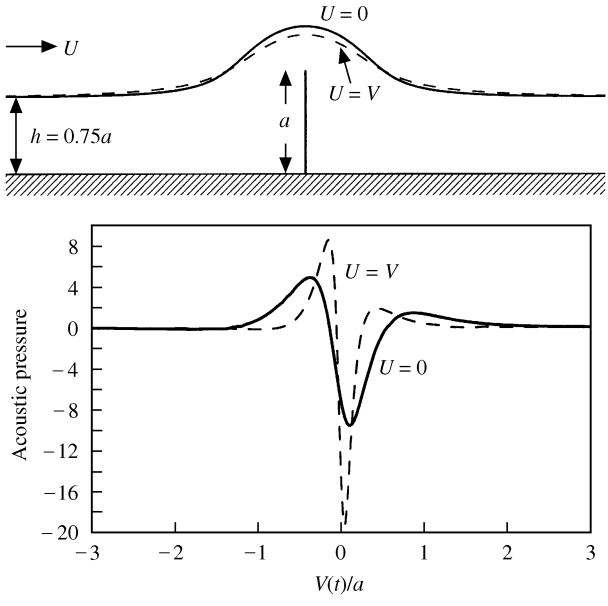


Figure 11. Vortex trajectories and non-dimensional farfield acoustic pressures (39) when $h/a = 0{\cdot}75$ for $U = 0$ (——) and $U = V \equiv \Gamma/4\pi a$ (- - - -).

the barrier where the interaction is strongest. The convection velocity at this point is also increased from about $1{\cdot}98V$ and $U = 0$ to $3{\cdot}95V$ when $U = V$, and this is responsible for more than doubling the amplitude of the sound and its effective frequency.

The inviscid wall barrier problem is dynamically equivalent to that in which a *vortex pair*, consisting of a vortex $\Gamma$ at $z_0$ accompanied by an "image" of strength $-\Gamma$ at $z_0^*$, is incident symmetrically and normally on a "vertical" rigid strip of width $2a$. It is now obvious that the net dipole strength in the vertical (i.e., $x_2$) direction (that we have previously attributed to suction forces at the edges) must vanish identically. The "doubling" of the drag dipole sound is then seen to be a consequence of the separate contributions to the overall sound from the vortex $\Gamma$ and its image.

## 6. VORTEX INTERACTING WITH A CIRCULAR CYLINDER

### 6.1. ISOLATED CYLINDER

The two-dimensional problem of a line vortex in motion near a parallel circular cylinder is one of the simplest examples of a bluff-body interaction. Let the cylinder have radius $a$ and be coaxial with the $x_3$-axis, and let there be an irrotational mean flow at speed $U$ past the cylinder in the $x_1$ direction, with no mean circulation about the cylinder.

Set $z = x_1 + \mathrm{i}x_2$ and let the vortex have the complex position $z_0 = x_{01} + \mathrm{i}x_{02}$ at time $t$. The complex potential $w(z)$ of the motion is found by placing an image vortex $-\Gamma$ at the inverse point $z = a/z_0^*$ and a vortex $+\Gamma$ at the center (as in the transformed plane of section 3). Taking account also of the potential for the uniform mean flow past the cylinder, we find [22]

$$w(z) = -\frac{\mathrm{i}\Gamma}{2\pi}\ln(z - z_0) + \frac{\mathrm{i}\Gamma}{2\pi}\ln\left(z - \frac{a^2}{z_0^*}\right) - \frac{\mathrm{i}\Gamma}{2\pi}\ln z + U\left(z + \frac{a^2}{z}\right). \tag{40}$$

The complex potential governing the motion of $\Gamma$ is now obtained by subtracting the self-potential $(-\mathrm{i}\Gamma/2\pi)\ln(z-z_0)$, following which we derive the vortex equation of motion

$$\frac{\mathrm{d}Z^*}{\mathrm{d}T} = \frac{\mathrm{i}}{Z(|Z|^2-1)} + \varepsilon\left(1-\frac{1}{Z^2}\right), \tag{41}$$

where

$$Z = z_0/a, \quad V = \Gamma/(2\pi a), \quad T = Vt/a, \quad \varepsilon = U/V, \quad \text{and} \quad \mathrm{d}z_0/\mathrm{d}t = V(\mathrm{d}Z/\mathrm{d}T) \equiv V(u+\mathrm{i}v).$$

The acoustic pressure is determined by equation (18), wherein the Kirchhoff vector for the cylinder has the components

$$Y_1 = \mathrm{Re}\left(z+\frac{a^2}{z}\right), \qquad Y_2 = \mathrm{Re}\left\{-\mathrm{i}\left(z-\frac{a^2}{z}\right)\right\}, \quad z = y_1 + \mathrm{i}y_2. \tag{42}$$

Set

$$\mathscr{W}_1 = \frac{\mathrm{d}}{\mathrm{d}z}\left(z+\frac{a^2}{z}\right) \equiv 1-\frac{1}{Z^2}, \qquad \mathscr{W}_2 = \frac{\mathrm{d}}{\mathrm{d}z}\left\{-\mathrm{i}\left(z-\frac{a^2}{z}\right)\right\} \equiv -\mathrm{i}\left(1+\frac{1}{Z^2}\right).$$

and make the change of integration variable $\hat{T} = V\tau/a$ in equation (18) to obtain the acoustic pressure in the form

$$p(\mathbf{x},t) \approx \frac{\rho_0 \Gamma V \sqrt{M} a^{1/2} x_j}{2\pi\sqrt{2c_0|\mathbf{x}|^{3/2}}} \frac{\partial}{\partial T} \int_{-\infty}^{[T]} \mathrm{Im}(\mathscr{W}_j(u+\mathrm{i}v))(\hat{T}) \frac{\mathrm{d}\hat{T}}{\sqrt{[T]-\hat{T}}},$$

where

$$M = V/c_0, \; [T] = (V/a)\,(t-|\mathbf{x}|/c_0).$$

The subscripts $j = 1, 2$, respectively, correspond to the acoustic pressures $p_1(\mathbf{x}, t)$, $p_2(\mathbf{x}, t)$ generated by the *drag* and *lift* dipoles, i.e., by the components of the unsteady force $(F_1, F_2)$ exerted on the fluid (per unit span) by the cylinder. The integrals must be evaluated numerically using the numerical solution of equation (41) for the path of the vortex. This is done by making the further change of integration variable $\lambda = \sqrt{[T]-\hat{T}}$, leading to

$$\frac{p_1(\mathbf{x},\,t)}{\rho_0 V^2 \sqrt{M}\sin\Theta(a/|\mathbf{x}|)^{1/2}} \approx 2^{1/2}\frac{\partial}{\partial T}\int_0^{\infty} \mathrm{Im}\,(\mathscr{W}_1(u+\mathrm{i}v))\,([T]-\lambda^2)\,\mathrm{d}\lambda,$$

$$\frac{p_2(\mathbf{x},\,t)}{\rho_0 V^2 \sqrt{M}\cos\Theta(a/|\mathbf{x}|)^{1/2}} \approx 2^{1/2}\frac{\partial}{\partial T}\int_0^{\infty} \mathrm{Im}\,(\mathscr{W}_2(u+\mathrm{i}v))\,([T]-\lambda^2)\,\mathrm{d}\lambda. \tag{43}$$

The calculation of the vortex trajectory begins at time $T'$, say, by taking the initial position of the vortex to be far upstream of the cylinder at $z_0 = -L + \mathrm{i}h$, where $L \gg a$ is sufficiently large so that the acoustic source strengths are negligible for $T < T'$ (Figure 12). The upper limits of integration in equation (43) are then finite, because the source terms vanish as soon as $[T]-\lambda^2 < T'$.

Figure 12 illustrates the typical non-dimensional waveforms (43) produced when $V \equiv \Gamma/2\pi a = 2U$ and for $h/a = \pm 0{\cdot}7$. The lift and drag dipole radiations are typically of the same order of magnitude. When $U \gg V$, the lift dipole will tend to predominate, because in this case convection by the image vortices can be neglected in a first approximation, and then the drag dipole source strength becomes $(\boldsymbol{\omega} \wedge U\nabla Y_1)\cdot\nabla Y_1 \equiv 0$. The figure shows how the amplitude of the sound decreases rapidly with increasing distance of closet approach of

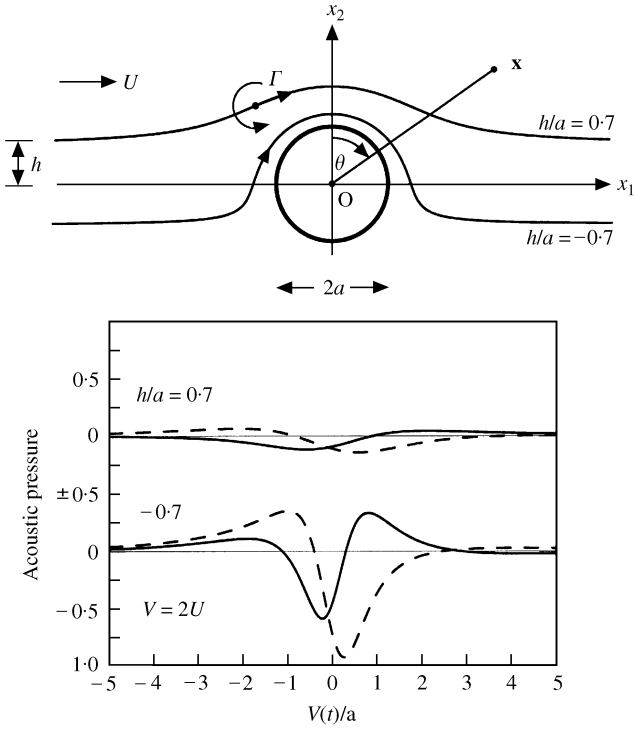


Figure 12. Vortex trajectories and non-dimensional acoustic pressures (43) when $h/a = \pm 0{\cdot}7$ for $V \equiv \Gamma/2\pi a = 2U$: —— lift dipole, $p_2$; - - - -, drag dipole, $p_1$.

the vortex to the cylinder; near the cylinder the translational velocity of the vortex is increased because the mean flow velocity is larger, and also because of the increased influence of the image vorticity.

When $U \gg V$, a vortex initially released far upstream with $h < 0$ will pass *below* the cylinder (as opposed to the case shown in the figure, where the induced velocity produced by image vorticity deflects the path to pass over the cylinder). In that case, however, the qualitative shapes of the pressure signatures are unchanged (provided $\Gamma$ remains positive). This can be understood by using definitions (42) to introduce "stream functions" $\Psi_1$, $\Psi_2$ that are, respectively, constant on the streamlines of the uniform flows past the cylinder determined by the velocity potentials $Y_1$, $Y_2$, i.e., where

$$Y_1 + \mathrm{i}\Psi_1 = z + \frac{a^2}{z}, \qquad Y_2 + \mathrm{i}\Psi_2 = -\mathrm{i}\left(z - \frac{a^2}{z}\right), \quad z = y_1 + \mathrm{i}y_2.$$

Then the drag and lift source strengths are, respectively, proportional to the retarded values of

$$\frac{\mathrm{D}\Psi_1}{\mathrm{D}t} \quad \text{and} \quad \frac{\mathrm{D}\Psi_2}{Dt}.$$

$\Psi_2$ always increases in the direction of motion of the vortex, independent of whether the vortex passes above or below the cylinder, so the lift source always has the same character. $\Psi_1$ is an odd function of $y_2$, and locally increases with increasing values of $y_2$; however, this source is not affected by the mean flow component of the convection velocity of the vortex,

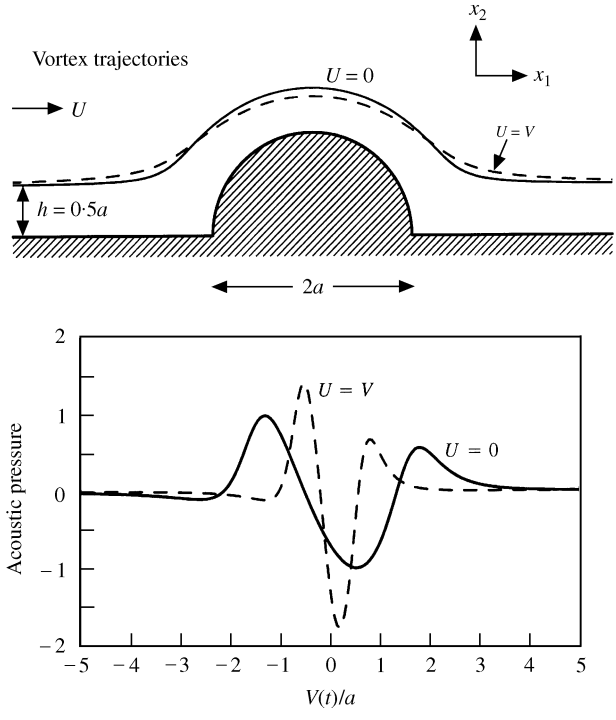


Figure 13. Vortex trajectories and non-dimensional farfield acoustic pressures (46) when $h/a = 0{\cdot}5$ for $U = 0$ (——) and $U = V \equiv \Gamma/2\pi a$ (- - - -).

only by the induced velocity of the image whose direction is such as to make $\mathrm{D}\Psi_1/\mathrm{D}t$ an even function of $y_2$.

### 6.2. WALL MOUNTED CYLINDER

The production of sound by a vortex translating past a cylindrical, semi-circular projection on a rigid wall (Figure 13) is analogous to the wall barrier of the problem of section 5. In inviscid flow, it is equivalent to the interaction of a *vortex pair*, the vortex of strength $\Gamma$ at $z_0$ plus its "image" of strength $-\Gamma$ at $z_0^*$, incident symmetrically on an isolated circular cylinder. Evidently, the symmetry implies that the lift dipole is null.

The velocity potential of the unsteady motion is obtained by augmenting the complex potential (40) by

$$\frac{\mathrm{i}\Gamma}{2\pi}\ln(z - z_0^*) - \frac{\mathrm{i}\Gamma}{2\pi}\ln\left(z - \frac{a^2}{z_0}\right) + \frac{\mathrm{i}\Gamma}{2\pi}\ln z.$$

Then

$$\frac{\mathrm{d}Z^*}{\mathrm{d}T} = \mathrm{i}\left\{\frac{1}{Z - Z^*} + \frac{Z - Z^*}{(|Z|^2 - 1)(Z^2 - 1)}\right\} + \varepsilon\left(1 - \frac{1}{Z^2}\right), \tag{44}$$

where

$$Z = z_0/a, \quad V = \Gamma/(2\pi a), \quad T = Vt/a, \quad \varepsilon = U/V.$$

The farfield acoustic pressure is given by equation (37), where

$$Y_1 = \mathrm{Re}\left(z + \frac{a^2}{z}\right). \tag{45}$$

The radiation is produced by the unsteady drag force exerted on the fluid by the cylinder, which vanishes in the linearized approximation, when the vortex is assumed to convect passively at the local velocity of the undisturbed mean stream. As before, set

$$\frac{\mathrm{d}Z}{\mathrm{d}T} = u(T) + \mathrm{i}v(T), \qquad \mathscr{W}_1 = \frac{\mathrm{d}}{\mathrm{d}z}\left(z + \frac{a^2}{z}\right) = 1 - \frac{1}{Z^2}$$

evaluated at the vortex. Then equations (37) and (45) yield

$$\frac{p_1(\mathbf{x},\ t)}{\rho_0 V^2 \sqrt{M} \sin\Theta (a/|\mathbf{x}|)^{1/2}} \approx 2^{3/2} \frac{\partial}{\partial T} \int_0^\infty \mathrm{Im}\,(\mathscr{W}_1\,(u + \mathrm{i}v))\,([T] - \lambda^2)\,\mathrm{d}\lambda, \tag{46}$$

where the angle $\Theta$ is defined as in Figure 12, $[T] = V[t]/a$ is the non-dimensional retarded time, and $M = V/c_0$.

The vortex path equation (44) and the acoustic pressure integral (46) must be evaluated numerically, taking the initial position of the vortex to be several cylinder radii $a$ upstream where its motion is unaffected by the presence of the cylinder. The upper part of Figure 13 shows the vortex trajectories when the initial stand-off distance of the vortex from the wall $h = 0{\cdot}5a$ for the two cases (1) of no mean flow, $U = 0$, and (2) $U = V$. The effect of mean flow is to draw the trajectory marginally closer to the cylinder as it passes over the top of the cylinder, where the vortex–surface interaction is strong. The convection velocity at this point is also increased from about $1{\cdot}23V$ when $U = 0$ to $3{\cdot}07V$ when $U = V$, and this is responsible for the increased acoustic amplitude and for more than doubling the effective frequency of the sound.The waveforms and these general conclusions are qualitatively the same as in the corresponding problem in Figure 11 for a vortex interacting with a thin wall barrier.

## 7. VORTEX INTERACTIONS WITH A RIGID SPHERE

A sphere represents the simplest three-dimensional bluff body whose inviscid interactions with simple vortex distributions are amenable to elementary analysis [25–32]. Knio *et al.* [32] have applied the method of matched asymptotic expansions to the problem of sound generation by a vortex ring interacting with a sphere at low Mach number. In this section, we shall investigate a simple version of their problem by direct application of the theory of vortex sound; we also discuss the case of a sphere interacting with a nominally rectilinear vortex.

### 7.1. SPHERE INTERACTING WITH A LINE VORTEX

The sound generated when a nominally rectilinear vortex is swept past a sphere can be treated in a linearized fashion, by assuming that each element of the vortex core is convected along a streamline of the undisturbed, steady mean flow at the local mean velocity. Consider a rigid sphere of radius $a$ with center at the co-ordinate origin in the presence of a steady *irrotational flow* which has speed $U$ in the $x_1$ direction when $|\mathbf{x}| \gg a$. The mean velocity at $\mathbf{x}$ is therefore

$$\mathbf{U} = U\nabla X_1(\mathbf{x}), \tag{47}$$

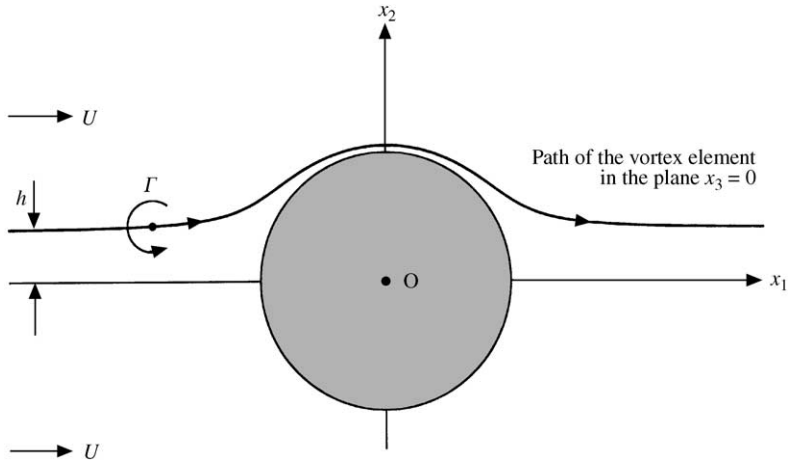


Figure 14. Illustration of the definition of the standoff distance $h$ and the path of the vortex element in the plane of symmetry ($x_3 = 0$) for a rectilinear vortex convected in a mean irrotational flow past the sphere.

where $X_1(\mathbf{x})$ is the $x_1$-component of the Kirchhoff vector for the sphere, which has the general representation

$$X_i = x_i \left(1 + \frac{a^3}{2|\mathbf{x}|^3}\right). \tag{48}$$

Consider a line vortex of strength $\Gamma$ that is initially far upstream of the sphere and parallel to the $x_3$-axis at a distance $h$ above the plane $x_2 = 0$. The vortex is convected towards the sphere by the mean flow. That part of the vortex that passes close to the sphere must evidently be deformed as it negotiates a passage around the sphere; more distant parts of the vortex that satisfy $|x_3| \gg a$ are largely unaffected by the sphere, and remain parallel to the $x_3$ direction during and after the interaction. The shape of the distorted vortex is symmetric with respect to the mid-plane $x_3 = 0$; the vortex element initially on $x_3 = 0$ remains on this plane of symmetry as it convects past the sphere along a mean streamline, as illustrated in Figure 14.

The shape of the vortex at time $t$ is determined by the solution of the equations

$$\frac{\mathrm{d}x_1}{\mathrm{d}t} = U\frac{\partial X_1}{\partial x_1}(\mathbf{x}), \quad \frac{\mathrm{d}x_2}{\mathrm{d}t} = U\frac{\partial X_1}{\partial x_2}(\mathbf{x}), \quad \frac{\mathrm{d}x_3}{\mathrm{d}t} = U\frac{\partial X_1}{\partial x_3}(\mathbf{x})$$

for each element of the vortex. If the undistorted sections of the vortex (at $|x_3| \gg a$) are taken to convect across the plane $x_1 = 0$ at time $t = 0$, these equations are to be integrated for each vortex element subject to the initial conditions

$$x_1 = -Ut, \quad x_2 = h, \quad x_3 = x_3^0 \quad t \to -\infty,$$

where $x_3^0$ is the initial "spanwise" location of the element.

By setting

$$T = \frac{Ut}{a}, \qquad \bar{\mathbf{x}} = \frac{\mathbf{x}}{a},$$

the equations of motion of a point on the vortex can be cast in the non-dimensional form

$$\frac{\mathrm{d}\bar{x}_1}{\mathrm{d}T} = 1 + \frac{\bar{x}_2^2 + \bar{x}_3^2 - 2\bar{x}_1^2}{2(\bar{x}_1^2 + \bar{x}_2^2 + \bar{x}_3^2)^{5/2}}, \quad \frac{\mathrm{d}\bar{x}_2}{\mathrm{d}T} = \frac{-3\bar{x}_1\bar{x}_2}{2(\bar{x}_1^2 + \bar{x}_2^2 + \bar{x}_3^2)^{5/2}}, \quad \frac{\mathrm{d}\bar{x}_3}{\mathrm{d}T} = \frac{-3\bar{x}_1\bar{x}_3}{2(\bar{x}_1^2 + \bar{x}_2^2 + \bar{x}_3^2)^{5/2}}.$$

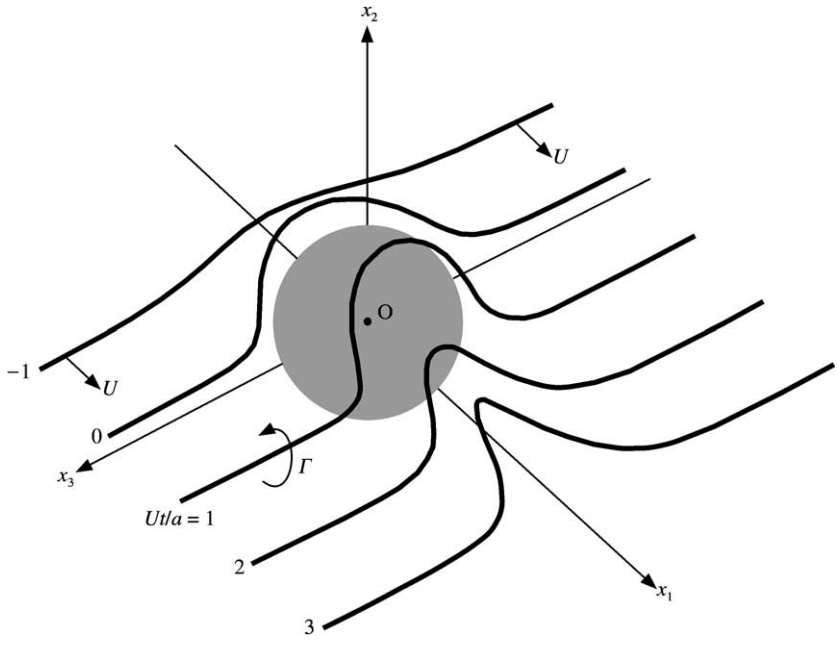


Figure 15. Stages in the linear theory distortion of a line vortex convected irrotationally in a mean flow past the sphere in the $x_1$ direction when $h/a = 0{\cdot}2$.

The integration can in practice start at time $T = -10$, say, with the vortex initially five diameters upstream of the sphere. It may safely by assumed that the sphere has no perceptible influence on vortex elements that initially satisfy $|\vec{x}_3^0| > 10$.

Figure 15 illustrates the calculated shape of the vortex line at different times $T = Ut/a$ when $h/a = 0{\cdot}2$, the vortex being convected over the upper surface of the sphere. The distortion of the vortex first becomes evident at about $T = -2$, and the figure depicts the progressively distorted forms at later times. The "hairpin" loop is produced because the translation velocities of vortex elements close to the sphere are small in the neighborhood of the "stagnation points" just in front and just to the rear of the sphere, causing the sides of the loop to be stretched to a length $\sim O(\ln(a/h))$ [26]; the accelerated motion over the upper surface of the sphere is insufficient to counteract the formation of the loop. In reality, of course, the motion would be strongly influenced by large self-induced velocities of the vortex [19], and by the production of additional vorticity by diffusion and separation from the surface [30, 31].

The sound generated during this inviscid interaction can be calculated using formula (10), where in

$$\mathbf{v} = U\nabla Y_1(\mathbf{y}).$$

There is no contribution to the integral in equation (10) from $j = 1$ (because $\nabla Y_1 \wedge \nabla Y_1 \equiv \mathbf{0}$); similarly, symmetry precludes the existence of a net "side-force" on the sphere, so that the subscript $j = 3$ also makes no contribution to the integral. The sound may therefore be attributed to a dipole source orientated in the $x_2$ direction, whose strength equals the unsteady force on the fluid in this direction. Thus, equation (10) supplies

$$p(\mathbf{x}, t) \approx \frac{-\rho_0 U \cos\Theta}{4\pi c_0 |\mathbf{x}|} \frac{\partial}{\partial t} \int (\boldsymbol{\omega} \cdot \nabla Y_1 \wedge \nabla Y_2) \left( \mathbf{y}, t - \frac{|\mathbf{x}|}{c_0} \right) \mathrm{d}^3 \mathbf{y}, \quad |\mathbf{x}| \to \infty, \tag{49}$$

where $\Theta = \cos^{-1}(x_2/|\mathbf{x}|)$ is the angle between the observer direction $\mathbf{x}$ an the $x_2$-axis.

The integral is evaluated by writing

$$\boldsymbol{\omega} = \Gamma\delta(\mathbf{s}_\perp)\hat{\mathbf{s}}, \qquad \mathrm{d}^3\mathbf{y} = \mathrm{d}^2\mathbf{s}_\perp\,\mathrm{d}s,$$

where

$$\hat{\mathbf{s}} = (\hat{s}_1, \hat{s}_2, \hat{s}_3) = \text{unit vector locally parallel to } \boldsymbol{\omega},$$

$\mathbf{s}_\perp$ is the vector distance measured in the normal direction from the local axis of the vortex, and $s$ is the distance measured along the vortex in the direction of $\boldsymbol{\omega}$. Then equation (49) becomes

$$\frac{p_1(\mathbf{x},\,t)}{\rho_0\Gamma UM\cos\Theta/4\pi|\mathbf{x}|} = -\frac{\partial}{\partial T}\int_{-\infty}^{\infty}[\hat{\mathbf{s}}\cdot\nabla Y_1 \wedge \nabla Y_2]\,\mathrm{d}\bar{s}, \quad \bar{s} = \frac{s}{a}, \quad M = \frac{U}{c_0}, \tag{50}$$

where the integrand is evaluated at the retarded position of the distorted vortex.

The integral in equation (50) is formally divergent, because

$$\hat{\mathbf{s}}\cdot\nabla Y_1 \wedge \nabla Y_2 \to 1 \quad \text{as} \quad \bar{s} \to \pm\infty\,.$$

The divergence is artificial, however, being a consequence of formal operations used in the application of the compact Green function (6). The "infinite" contributions to the integral from large values of $\bar{s}$ are constant at successive retarded locations of the vortex, and disappear on differentiation with respect to $T$. The integral can therefore be evaluated numerically by restricting the range of integration to a finite interval, say, $-10 < \bar{s} < 10$, because the contributions at larger values of $\bar{s}$ are the same for all retarded times, and give no contribution to the sound on differentiation.

Typical plots of the non-dimensional pressure predicted by equation (50) are shown in Figure 16 for $h/a = 0{\cdot}2$, $0{\cdot}8$; they illustrate the decrease in the sound level with increasing values of the initial standoff distance $h$ of the vortex. The pressure signatures are consistent with the lift dipole radiation in Figures 8 and 9 for an airfoil of compact span (vortex shedding is responsible for the absence of a secondary, negative peak in the airfoil results). In practice, of course, the gross distortion of the vortex evident in Figure 15 will be accompanied by self-induced vortex motions that will tend to modify the details of the predicted surface interaction noise. These motions can also generate conventional

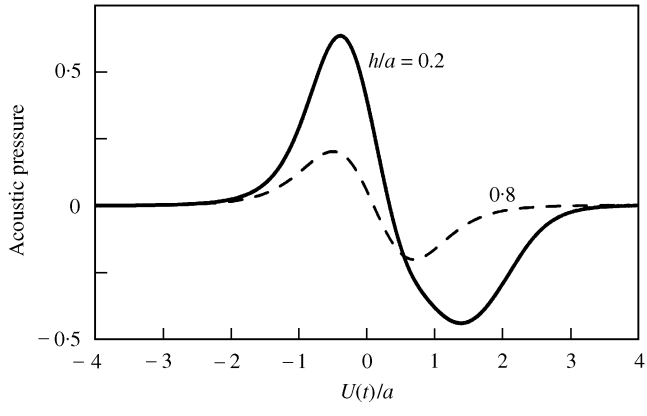


Figure 16. Linear theory prediction (50) of the sound produced during the convection of a line vortex past the sphere for $h/a = 0{\cdot}2$ (——)and $= 0{\cdot}8$ (- - - -).

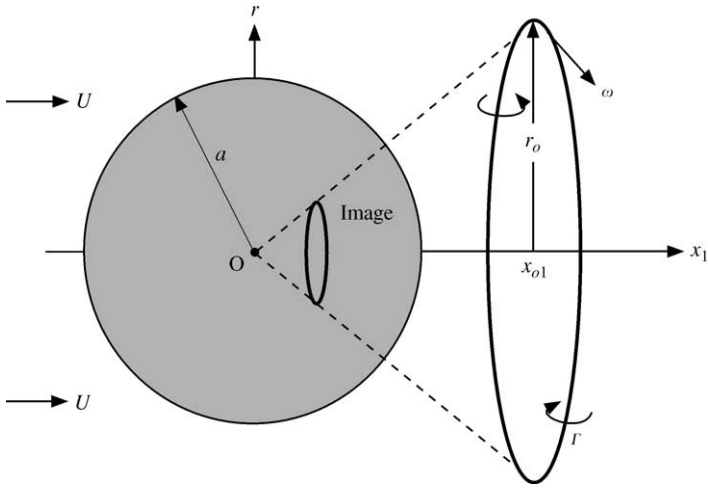


Figure 17. Configuration of the vortex ring and its image in the sphere.

"quadrupole noise", independent of the presence of the sphere, but its relative intensity at low Mach numbers would be expected to be small, at least at the dominant frequencies of the unsteady motion.

### 7.2. VORTEX RING INTERACTING WITH A SPHERE

Consider next a vortex ring of radius $r_0(t)$ and circulation $\Gamma$ which is coaxial with the $x_1$-axis and which translates in the positive $x_1$ direction under the influence of *self-induction* and the mean flow past the sphere (Figure 17). Suppose the vortex core to be circular and of radius $\sigma \ll r_0$, and neglect any distortion of the core by interaction with the sphere. Then the self-induced velocity $u_\Gamma$ of the vortex (in inviscid flow) is given by Kelvin's formula [19, 25]

$$u_\Gamma(r_0, \sigma) = \frac{\Gamma}{4\pi r_0}\left\{\ln\left(\frac{8r_0}{\sigma}\right) - \frac{1}{4}\right\}. \tag{51}$$

The influence of the sphere on the motion is accounted for by a coaxial image ring vortex whose circulation $\Gamma'$, radius $r_0'$ and axial location $x_{01}'$ are given by [25, 30]

$$\Gamma' = -\frac{\Gamma(r_0^2 + x_{01}^2)^{1/2}}{a}, \qquad r_o' = \frac{a^2 r_o}{r_0^2 + x_{01}^2}, \qquad x_{01}' = \frac{a^2 x_{01}}{r_0^2 + x_{01}^2}, \tag{52}$$

where $x_{01}$ is the intersection of the plane of symmetry of the vortex with the $x_1$-axis. The combined velocity of motion of the vortex induced by this image and by the irrotational mean flow past the sphere can be expressed in terms of Stokes stream function $\psi(r, x_1)$, which has the form [19, 25]

$$\psi(r, x_1) = -\frac{Ur^2}{2}\left(1 - \frac{a^3}{(r^2 + x_1^2)^{3/2}}\right) - \frac{\Gamma'}{2\pi}(\Re_+ + \Re_-)\{K(\Lambda) - E(\Lambda)\}, \tag{53}$$

where

$$\mathfrak{R}_{\pm} = \sqrt{(r \mp r_0')^2 + (x_1 - x_{01}')^2}, \qquad \Lambda = \frac{\mathfrak{R}_- - \mathfrak{R}_+}{\mathfrak{R}_- + \mathfrak{R}_+},$$

$$K(\Lambda) = \int_0^{\pi/2} \frac{\mathrm{d}\mu}{\sqrt{1 - \Lambda^2 \sin^2 \mu}}, \qquad E(\Lambda) = \int_0^{\pi/2} \sqrt{1 - \Lambda^2 \sin^2 \mu}\, \mathrm{d}\mu,$$

and where $r$ denotes perpendicular distance from the $x_1$-axis, and $K(\Lambda)$, $E(\Lambda)$ are, respectively, complete elliptic integrals of the first and second kinds.

The radius $r_0(t)$ and axial position $x_{01}(t)$ of the vortex ring are then determined by the equations of motion

$$\frac{\mathrm{d}r_0}{\mathrm{d}t} = \frac{1}{r_0}\frac{\partial \psi}{\partial x_1}(r_0, x_{01}), \qquad \frac{\mathrm{d}x_{01}}{\mathrm{d}t} = u_\Gamma(r_0, \sigma) - \frac{1}{r_0}\frac{\partial \psi}{\partial r}(r_0, x_{01}). \tag{54}$$

The radius $\sigma$ of the vortex core decreases when $r_0$ increases, because the vortex lines move with the fluid particles. If $h$ denotes the radius $r_0$ of the vortex at large distances from the sphere, and $\sigma_0$ is the corresponding core radius, then at time $t$,

$$(2\pi r_0)\pi\sigma^2 = (2\pi h)\pi\sigma_0^2, \quad \text{i.e., } \sigma(t) = \sigma_0\sqrt{\frac{h}{r_0}}$$

and the self-induction velocity (51) is given in terms of the current radius $r_0(t)$ by the formula

$$u_\Gamma = \frac{\Gamma}{4\pi r_0}\left\{\ln\left(\frac{8h}{\sigma_0}\left[\frac{r_0(t)}{h}\right]^{3/2}\right) - \frac{1}{4}\right\}. \tag{55}$$

The equations of motion are cast in non-dimensional terms by defining

$$X = \frac{x_{01}}{a}, \qquad R = \frac{r_0}{a}, \qquad V = \frac{\Gamma}{2\pi a}, \qquad T = \frac{Vt}{a}, \qquad \varepsilon = \frac{U}{V}.$$

Then

$$\frac{\mathrm{d}R}{\mathrm{d}T} = \frac{1}{R}\frac{\partial \Psi}{\partial X}(R, X), \qquad \frac{\mathrm{d}X}{\mathrm{d}T} = -\frac{1}{R}\frac{\partial \Psi}{\partial X}(R, X) + \frac{1}{2R}\left\{\ln\left(\frac{8h}{\sigma_0}\left[\frac{aR}{h}\right]^{3/2}\right) - \frac{1}{4}\right\}, \tag{56}$$

where

$$\Psi = -\frac{\varepsilon R^2}{2}\left(1 - \frac{1}{(R^2 + X^2)^{3/2}}\right) + (R^2 + X^2)^{1/2}(\hat{\mathfrak{R}}_+ + \hat{\mathfrak{R}}_-)\{K(\Lambda) - E(\Lambda)\},$$

$$\hat{\mathfrak{R}}_{\pm} = \sqrt{(R \mp R')^2 + (X - X')^2}, \qquad \Lambda = \frac{\hat{\mathfrak{R}}_- - \hat{\mathfrak{R}}_+}{\hat{\mathfrak{R}}_- + \hat{\mathfrak{R}}_+},$$

$$R' = \frac{R}{R^2 + X^2}, \qquad X' = \frac{X}{R^2 + X^2}.$$

Figure 18 illustrates the sections in the vertical plane of symmetry of the sphere of two typical vortex trajectories predicted by equations (56). In both cases, the integration is started at $X = -10$ (10 sphere radii) upstream with the following initial values for the vortex ring radius and core radius:

$$h = 0{\cdot}8a, \qquad \sigma_0 = 0{\cdot}05h. \tag{57}$$

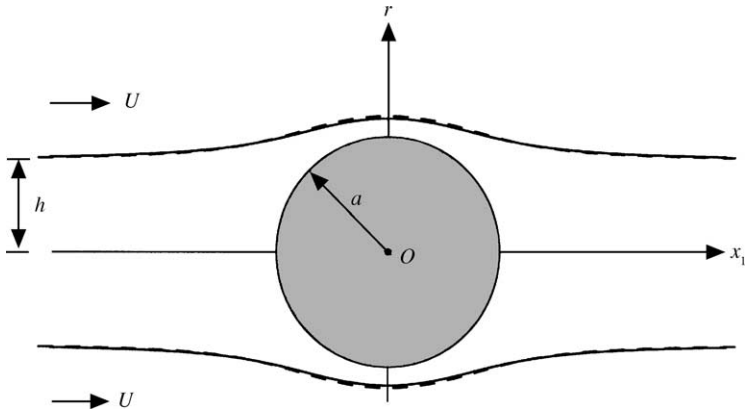


Figure 18. Vortex ring trajectories past the sphere when $h/a = 0{\cdot}8$, $\sigma_0 = 0{\cdot}05h$ for $\varepsilon = 0$ $(U = 0)$ (——) and $\varepsilon = 3$ (- - - -).

The solid and broken-like curves in the figure correspond, respectively, to $\varepsilon = 0$ (no mean flow) and $\varepsilon = 3$. The latter value is chosen to make the mean stream velocity $U$ approximately the same as the self-induced velocity $u_\Gamma$ at large distances from the sphere. This is seen to have a relatively small effect on the profile of the trajectory, expanding it slightly close to the sphere, although the speed of convection of the ring past the sphere is greatly increased.

The sound pressure radiated during the interaction is given in integral form by equation (10). To evaluate the integral, the finite size of the core diameter can be ignored, and the vorticity approximated by

$$\boldsymbol{\omega} = \Gamma\hat{\boldsymbol{\theta}}\delta(r - r_0(t))\,\delta(x_1 - x_{01}(t)), \tag{58}$$

where $\hat{\boldsymbol{\theta}}$ is a unit azimuthal vector, locally tangential to the vorticity $\boldsymbol{\omega}$ and orientated in the *clockwise* direction when the vortex ring is viewed from upstream, as indicated in Figure 17.

Because of the symmetry of the interaction, the unsteady force on the sphere must be in the mean flow direction; the sound is therefore produced by the unsteady *drag*, and only the component

$$Y_1 = y_1\left(1 + \frac{a^3}{2|\mathbf{y}|^3}\right) \equiv y_1\left(1 + \frac{a^3}{2(r^2 + y_1^2)^{3/2}}\right)$$

of the Kirchhoff vector can make a non-trivial contribution to equation (10). The production of sound is a *non-linear* event, dependent on the self-induced motion of the vortex and induction by the image vortex, because the contribution by convection by the mean velocity $U\nabla Y_1$ is null, since

$$(\boldsymbol{\omega} \wedge U\nabla Y_1)\left(\mathbf{y}, t - \frac{|\mathbf{x}|}{c_0}\right) \cdot \nabla Y_1(\mathbf{y}) \equiv 0.$$

Thus, substituting equation (50) into equation (10) and evaluating the integral, and expressing this result in non-dimensional form, we have

$$\frac{p(\mathbf{x}, t)}{\rho_0 V^2 M \cos\Theta(a/|\mathbf{x}|)} \approx \pi\frac{\partial}{\partial T}\left[\frac{3R^2X}{2(R^2 + X^2)^{5/2}}\frac{\mathrm{d}X}{\mathrm{d}T} + \left(1 + \frac{R^2 - 2X^2}{2(R^2 + X^2)^{5/2}}\right)R\frac{\mathrm{d}R}{\mathrm{d}T}\right], \tag{59}$$

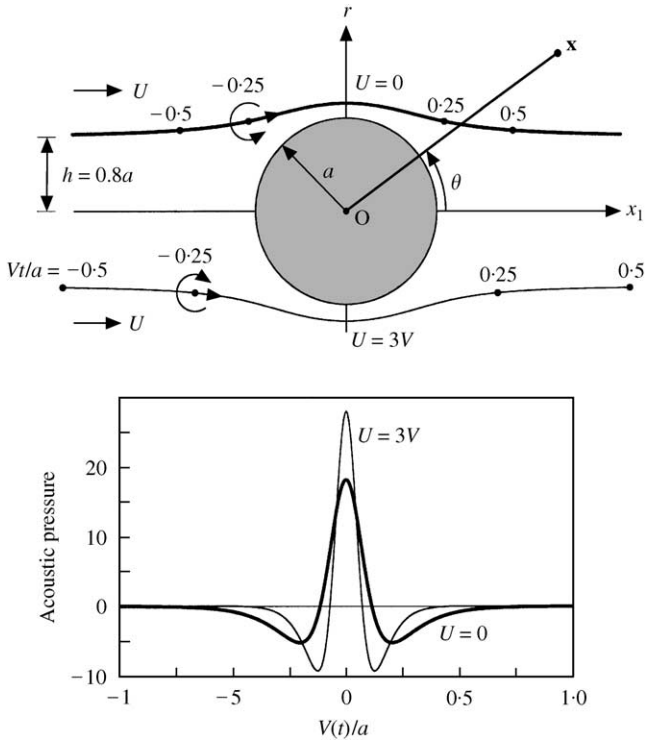


Figure 19. Retarded locations of the vortex ring and the corresponding acoustic pressure (59) when $h/a = 0{\cdot}8$, $\sigma_0 = 0{\cdot}05h$ for $\varepsilon = 0$ ($U = 0$) (———) and $\varepsilon = 3$ (——)..

where $M = V/c_0 \equiv \Gamma/2\pi ac_0$, and $R$ and $X$ are the solutions of equations (54). The term in square braces is evaluated at the retarded position of the vortex ring, and $\Theta$ is the angle between the radiation direction and the $x_1$-axis illustrated in the upper part of Figure 19.

The non-dimensional acoustic pressure signatures plotted in Figure 19 are for the same conditions considered above for the vortex ring trajectories and initial conditions (57) (see Figure 18). The thick solid curve is the pressure profile in the absence of mean flow ($U = 0$). The location of the vortex ring in this case at various retarded times $V[t]/a$ is indicated on the thick curve in the upper part of Figure 19. Similarly, the thin-line curves in the figure give the pressure and retarded positions for $U = 3V$, when the self-induction velocity $u_\Gamma \approx U$ at large distances from the sphere. Both the amplitude and frequency of the sound are increased because of the increased convection velocity of the vortex past the sphere.

## 8. VORTEX PAIR INCIDENT ON A THIN-WALL APERTURE

Hydrodynamic motion in the vicinity of an aperture in a large thin-wall generally produces an unsteady volume flux through the aperture which is acoustically equivalent to a monopole source, provided the aperture diameter is compact. The upper part of Figure 20 depicts a simple model of such a source. The rigid wall $x_1 = 0$ is pierced by a two-dimensional "slit" of width $2a$ whose centerline extends along the $x_3$-axis. A vortex pair

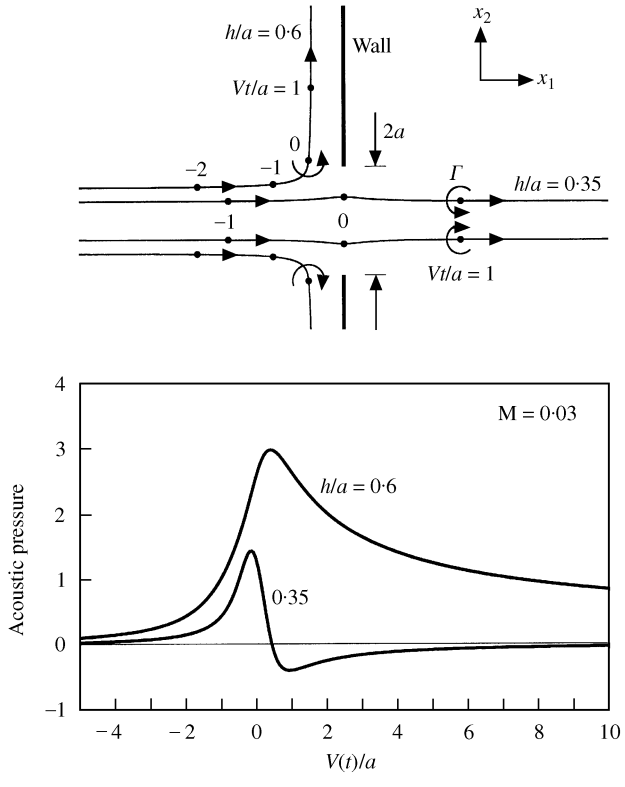


Figure 20. Trajectories and acoustic pressures (62) for a vortex pair approaching a wall aperture for $h/a = 0{\cdot}35$, $0{\cdot}6$; the sound is weakly dependent on the Mach number $M = \Gamma/4\pi a c_0$, and results are plotted for $M = 0{\cdot}03$.

aligned with the $x_3$-axis, consisting of vortices of strengths $\pm \Gamma$ at the respective complex conjugate positions $z_0 = x_{01} + \mathrm{i}x_{02}$ and $z_0^* = x_{01} - \mathrm{i}x_{02}$ impinges on the aperture from the "left" ($x_1 = -\infty$).

The motion is symmetric with respect to the $x_2$-axis, and the transformation [22]

$$\zeta = \frac{z}{\sqrt{z^2 + a^2}}, \qquad z = x_1 + \mathrm{i}x_2,$$

maps the region $\mathrm{Im}\, z > 0$ cut along the upper section $x_2 > a$ of the wall onto the upper-half of the $\zeta$-plane. This permits the equation of motion of the vortex pair to be determined in the form

$$\frac{\mathrm{d}Z^*}{\mathrm{d}T} = \frac{3\mathrm{i}Z}{Z^2 + 1} + \frac{2\mathrm{i}}{(Z^2 + 1)^{3/2}\{Z/\sqrt{Z^2 + 1} - (Z/\sqrt{Z^2 + 1})^*\}}, \tag{60}$$

where $Z = z_0/a$, $T = Vt/a$, $V = \Gamma/(4\pi a)$ and $\mathrm{d}z_0/\mathrm{d}t = V\,(\mathrm{d}Z/\mathrm{d}T) \equiv V(u + \mathrm{i}v)$.

Let the initial separation of the vortices at $x_1 = -\infty$ be $2h$. To integrate equation (60), we set $z_0 = -L + \mathrm{i}h$ at a convenient initial (but arbitrary) time $T = T'$, where $L \gg a$. When $h/a$ is smaller than $\frac{2}{3}^{3/2} \sim 0{\cdot}385$ [33], the vortex pair passes through the aperture in the manner indicated in Figure 20 for $h/a = 0{\cdot}35$. For larger values of $h/a$, the trajectories of the two vortices separate and follow symmetric paths parallel to the wall on either side of the aperture, as illustrated for $h/a = 0{\cdot}6$.

The acoustic pressure for an arbitrary inviscid, vortex–surface interaction at low Mach numbers is given by the first integral on the right of equation (5). When the width $2a$ of the aperture is small compared to the characteristic acoustic wavelength of the sound, the appropriate compact Green function assumes the form [4, 34]

$$G(\mathbf{x}, \mathbf{y}, t-\tau) \approx -\frac{\sqrt{c_0 \operatorname{sgn}(x_1)}}{\pi\sqrt{2\pi|\mathbf{x}|}} \frac{\chi(t-\tau-|\mathbf{x}|/c_0)}{\sqrt{t-\tau-|\mathbf{x}|/c_0}} \operatorname{Re}\left\{\ln\left(\frac{\tilde{z}}{a}+\sqrt{\frac{\tilde{z}^2}{a^2}-1}\right)\right\}, \quad \tilde{z} = y_2 + \mathrm{i}y_1, \tag{61}$$

where

$$\chi(t) = \begin{cases} 0, & t < 0, \\ \displaystyle\int_0^\infty \frac{\ln(\varpi u \xi^2/4c_0 t)\, \mathrm{e}^{-\xi^2}\, \mathrm{d}\xi}{[\ln(\varpi a \xi^2/4c_0 t)]^2 + \pi^2}, & t > 0; \end{cases} \qquad \varpi = 1{\cdot}781072.$$

The dependence on source position $\mathbf{y}$ in equation (61) is contained entirely in the logarithmic term, which represents the velocity potential of the ideal flow that would be produced through the aperture (from "left" and "right") by a uniform pressure drop across the wall.

When vortex shedding from the aperture edges is ignored, the vorticity is

$$\boldsymbol{\omega} = \Gamma \mathbf{k}\delta(y_1 - x_{01})\delta(y_2 - x_{02}) - \Gamma \mathbf{k}\delta(y_1 - x_{01})\delta(y_2 + x_{02}),$$

where $\mathbf{k}$ is a unit vector in the $x_3$ direction (out of the plane of the paper in Figure 20). Thus, defining

$$\tilde{\mathscr{W}}(Z) = \left(\frac{1}{\sqrt{\tilde{Z}^2 - 1}}\right)_{\tilde{Z} = \mathrm{i}Z^*}, \qquad \hat{\chi}(T) = \chi(t), \qquad M = \frac{V}{c_0},$$

and setting $\hat{T} = V\tau/a$, we find

$$p(\mathbf{x}, t) \approx \frac{2^{5/2}\rho_0 V^2 \operatorname{sgn}(x_1)}{\sqrt{\pi M}} \left(\frac{a}{|\mathbf{x}|}\right)^{1/2} \int_{-\infty}^{[T]} \operatorname{Re}(\tilde{\mathscr{W}}^*(Z)(u+\mathrm{i}v))(\hat{T}) \frac{\hat{\chi}([T]-\hat{T})\, \mathrm{d}\hat{T}}{\sqrt{[T]-\hat{T}}}, \quad [T] = \frac{V[t]}{a}.$$

Therefore, putting $\lambda = \sqrt{[T]-\hat{T}}$, the non-dimensional acoustic pressure is given by

$$\frac{p(\mathbf{x}, t)}{\rho_0 V^2 \operatorname{sgn}(x_1)(a/|\mathbf{x}|)^{1/2}} \approx \frac{2^{7/2}}{\sqrt{\pi M}} \int_0^\infty \operatorname{Re}(\tilde{\mathscr{W}}^*(Z)(u+\mathrm{i}v))\, ([T]-\lambda^2)\, \hat{\chi}(\lambda^2)\, \mathrm{d}\lambda, \quad |\mathbf{x}| \to \infty, \tag{62}$$

where

$$\hat{\chi}(\lambda^2) = \int_0^\infty \frac{\ln(\varpi M \xi^2/4\lambda^2)\, \mathrm{e}^{-\xi^2}\, \mathrm{d}\xi}{[\ln(\varpi M \xi^2/4\lambda^2)]^2 + \pi^2}.$$

For numerical purposes, the upper limit of integration in equation (62) is $\lambda = \sqrt{[T]-T'}$, where $T'$ is the non-dimensional initial time from which the motion of the vortex pair is calculated.

The value of the integral (62) depends weakly on the characteristic Mach number $M = V/c_0 \equiv \Gamma/4\pi a c_0$. This is just the *initial* value of the vortex convection Mach number (as $x_1 \to -\infty$) when the separation distance of the vortices $2h$ is the same as the width $2a$ of the aperture. We have taken $M = 0{\cdot}03$ for the farfield acoustic pressure signatures plotted in Figure 20; in air this would imply that $V \sim 10$ m/s.

The flow induced by the vortex pair approaching the wall forms a localized two-dimensional "jet" between the vortices, directed towards the wall. The resistance of the wall to this flow causes the pressure just to the left of the wall aperture to rise, forcing fluid through the aperture into the region $x_1 > 0$. The radiation therefore has the characteristics of an acoustic monopole source for $x_1 > 0$ and a sink for $x_1 < 0$. Numerical results are illustrated in the figure for $h/a = 0{\cdot}35, 0{\cdot}6$. In each case, the time origin has been adjusted to correspond approximately with the peak in the radiated acoustic pressure, which occurs when the vortices pass by the edges of the aperture. When $h/a = 0{\cdot}6$, the vortices do not penetrate the aperture but are deflected by the wall; this produces a relatively larger pressure rise than for $h/a = 0{\cdot}35$, where the vortices pass through the aperture. The maximum acoustic pressure amplitude is found to occur when $h/a$ just exceeds the critical value ( $\sim 0{\cdot}385$), when the vortex trajectories pass very close to the aperture edges.Further increases of $h/a$ beyond 0·6 result in a gradual reduction in the amplitude of the sound, and a corresponding increase in the width of the acoustic pulse (i.e., a decrease in the characteristic frequency of the sound).

## 9. CONCLUSION

The sound produced when unsteady flow interacts with an acoustically compact rigid surface (or surface element) is determined principally by the unsteady force between the surface and the fluid. Curle's [16] theory determines this force as a surface integral of the surface pressure. However, vortex methods are increasingly being recognized as an efficient tool for calculating the local unsteady flows in such interactions, and the theory of vortex sound provides an effective means of computing surface forces directly from a knowledge of the vorticity distribution and its evolution. The relative simplicity of this approach has been illustrated in this paper by consideration of a collection of vortex–surface interaction problems that can be solved for both the fluid motion and the generated sound by elementary numerical means. These solutions provide qualitative and quantitative insight into the mechanisms responsible for sound production, and also form the basis of a fundamental database that can be used to validate predictions of more general numerical schemes.

## REFERENCES

1. M. J. LIGHTHILL 1952 *Proceedings of the Royal Society of London, Series* A **211**, 564–587. On sound generated aerodynamically. Part I: General theory.
2. A. POWELL 1961 *University of California, Los Angeles Report No.* 61–70. Vortex sound.
3. M. S. HOWE 1975 *Journal of Fluid Mechanics* **71**, 625–673. Contributions to the theory of aerodynamic sound, with application to excess jet noise and the theory of the flute.
4. M. S. HOWE 1998 *Acoustic of Fluid–Structure Interactions.* Cambridge: Cambridge University Press.
5. M. J. LIGHTHILL 1963 in *Laminar Boundary Layers* (L. Rosenhead, editor). Oxford: Oxford University Press; Chapters 1 and 2.
6. A. J. CHORIN 1998 *Vorticity and Turbulence.* New York: Springer-Verlag; corrected edition.
7. G.-H. COTTET and P. D. KOUMOUTSAKOS 2000 *Vortex Methods: Theory and Practice.*Cambridge: Cambridge University Press.
8. H.-M. LENT, K. F. LOHER, G. E. A. MEIER and U. SCHIEVELBUSCH 1989 *Journal d'Acoustique* **2**, 365–367. Some processes of sound generation in a vortex–airfoil system with parallel axes.
9. S. LEE and D. BERSHADER 1994 *American Institute of Aeronautics and Astronautics Journal* **32**, 16–22. Head-on parallel blade–vortex interaction.
10. R. SEN 1997 *American Institute of Aeronautics and Astronautics Journal* **35**, 441–449. Vortex-oscillation model of airfoil side-edge noise.

11. C-H. KUO and J. K. HSIEH 1998 *Journal of Aircraft* **35**, 739–747. Parallel interaction of incident vortex array with oscillating airfoil.
12. N.W. M. KO, R. C. K. LEUNG and K. K. LAM 2000 *American Institute of Aeronautics and Astronautics Journal* **38**, 79–86. Two interacting vortex ring pairs and their sound generation.
13. T. H. WOOD and S. M. GRACE 2000 *American Institute of Aeronautics and Astronautics Paper AIAA*-0607. Free-wake analysis for calculating the aeroacoustics of a wing-flap configuration.
14. D. G. CRIGHTON 1985 *Annual Reviews of Fluid Mechanics* **17**, 411–445. The Kutta condition in unsteady flow.
15. W. R. SEARS 1941 *Journal of the Aeronautical Sciences* **8**, 104–108. Some aspects of non-stationary airfoil theory and its practical applications.
16. L. D. LANDAU and E. M. LIFSHITZ 1987 *Fluid Mechanics*. Oxford: Pergamon; second edition.
17. D. G. CRIGHTON, A. P. DOWLING, J. E. FFOWCS WILLIAMS, M. HECKL and F. G. LEPPINGTON 1992 *Modern Methods in Analytical Acoustics* (*Lecture Notes*). London: Springer-Verlag.
18. N. CURLE 1955 The influence of solid boundaries upon aerodynamic sound. *Proceedings of the Royal Society of London, Series A* **231**, 505–514.
19. G. K. BATCHELOR 1967 *An Introduction to Fluid Dynamics*. Cambridge: Cambridge University Press.
20. J. HADAMARD 1952 *Lectures on Cauchy's Problem in Linear Partial Differential Equations*. New York: Dover Publications.
21. M. S. HOWE 1989 *Journal of Fluid Mechanics* **206**, 131–153. On unsteady surface forces, and sound produced by the normal chopping of a rectilinear vortex.
22. L. M. MILNE-THOMSON 1968 *Theoretical Hydrodynamics*. London: Macmillan; fifth edition.
23. T. H. WOOD 2001 *Doctoral Thesis, Boston University*. Aerodynamic sound generated by a wing of complex geometry.
24. S. G. KASOEV 1976 *Soviet Physics Acoustics* **22**, 71–72. Sound radiation from a linear vortex over a plane with a projecting edge.
25. H. LAMB 1932 *Hydrodynamics*. Cambridge: Cambridge University Press; sixth edition.
26. M. J. LIGHTHILL 1956 Drift. *Journal of Fluid Mechanics* **1**, 31–53.
27. M. J. LIGHTHILL 1956 *Proceedings of the Cambridge Philosophical Society* **52**, 317–321. The image system of a vortex element in a rigid sphere.
28. H.-C. WANG 1970 *Annual Report of the Institute of Physics, Academia Sinica, Taiwan* 85–93. The motion of a vortex ring in the presence of a rigid sphere.
29. M. R. DHANAK 1981 *Journal of Fluid Mechanics* **110**, 129–147. Interaction between a vortex filament and an approaching rigid sphere.
30. L. TING and R. KLEIN 1991 in *Lecture Notes in Physics* Vol. 374. New York: Springer-Verlag. Viscous vortical flows.
31. G. PEDRIZZETTI 1992 *Journal of Fluid Mechanics* **245**, 701–722. Close interaction between a vortex filament and a rigid sphere.
32. O. M. KNIO, L. TING and R. KLEIN 1998 *Journal of the Acoustical Society of America* **103**, 83–98. Interaction of a slender vortex with a rigid sphere: dynamics and far field sound.
33. M. KARWEIT 1975 *Physics of Fluids* **18**, 1604–1606. Motion of a vortex pair approaching an opening in a boundary.
34. R. C. DUNNE and M. S. HOWE 1997 *Journal of Sound and Vibration* **202**, 605–618. Wall-bounded blade–tip vortex interaction noise.